

TABLE 1: Association between rainfall and *Giardia* prevalence: average seasonal rainfall in the study region (Indian Meteorological Department Database), average *Giardia* detection rates, and the percentage of Giardiasis among all diarrheal cases.

| Season               | Average rain (mm) | Monthly average <i>G. duodenalis</i> -positive cases | Total diarrhea cases | Monthly average <i>G. duodenalis</i> -positive (%) |
|----------------------|-------------------|--|----------------------|--|
| Premonsoon/summer 08 | 153.4             | 11   | 73                   | 15.05  |
| Monsoon 08           | 1291.7            | 12.75  | 103.5                | 12.02  |
| Postmonsoon 08       | 70.3              | 12   | 110.3                | 10.1   |
| Winter 09            | 3.4               | 4.5  | 91                   | 4.8  |
| Premonsoon/summer 09 | 251.8             | 11.7   | 123                  | 9.26   |
| Monsoon 09           | 971.5             | 18.75  | 141                  | 13.5   |
| Postmonsoon 09       | 95.7              | 5.7  | 73.3                 | 7.73   |
| Winter 10            | 16.6              | 2  | 34                   | 6.3  |
| Premonsoon/summer 10 | 143.7             | 7.3  | 67                   | 10.83  |
| Monsoon 10           | 787.4             | 4  | 48.25                | 8.32   |
| Postmonsoon 10       | 138.8             | 4.7  | 48                   | 10.3   |
| Winter 11            | 5.4               | 4  | 37.5                 | 10.7   |
| Premonsoon/summer 11 | 245.2             | 5  | 51.7                 | 10.03  |
| Monsoon 11           | 1391.6            | 1.75   | 35.5                 | 4.87   |
| Postmonsoon 11       | 29.5              | 2.7  | 32                   | 9.6  |

possible seasonality in *Giardia* prevalence. The percentage of *G. duodenalis*-positive cases detected was similar over the entire period with an average detection rate of around 10% each month (Figure 2(a)) and showed a significant correlation with the total number of diarrheal cases in each month ( $P < 0.001$ ). It was evident that the total number of diarrhea cases decreased significantly towards the end of the survey, a trend similar to that observed with *Giardia*-positive cases (Figures 2(a) and 2(b)). *G. duodenalis* showed a statistically significant seasonality and strong association with the total number of diarrheal cases ( $P = 0.001$ ); however, no significant association was found between the numbers of *Giardia*-positive cases and rainfall in the region ( $P > 0.05$ ) (see Supplementary File 1 available online at <http://dx.doi.org/10.1155/2014/786480>) (Table 1). The number of *Giardia* cases increased during the midsummer to monsoon season (i.e., from May to August). Seventy-four percent of the *Giardia*-positive cases were found to be coinfecting with other pathogens, while the remainders were single infections. As per the literature, *Giardia duodenalis* infection may not be associated with diarrhea or related diseases in some cases and rather remain asymptomatic for a long period of time [16, 17], but twenty-six percent of sole infection in the diarrhea patient among the study population demonstrates the symptomatic nature of *Giardia* in this case. Coinfection with *Vibrio cholerae* was the most common (32%), followed by rotavirus (19%) (Figure 3(a)). As all the tests for *Giardia* and other pathogens were conducted over the same set of samples, so the chance of generating data artifact was minimized and the multiple infection could be considered as true coinfection. Infection with *Giardia* showed a strong positive relationship with the presence of other diarrheal-causing pathogens ( $P < 0.001$ ) (Figure 3(b)). *Giardia* infection was very common in the lower age groups and statistically significant associations

TABLE 2: Multinomial logistic regression models exploring the significant predominant risk age group for *Giardia duodenalis* infection at IDBG, Kolkata (November 2007–July 2012).

| Age in years           | <i>Giardia duodenalis</i> | B     | OR (95% CI)        | P value |
|------------------------|---------------------------|-------|--------------------|---------|
| ≤5 years (n = 960)     | 144                       | 0.56  | 1.74 (1.29–2.35)   | <0.001* |
| >5–10 years (n = 126)  | 35                        | 1.33  | 3.79 (2.40–6.00)   | <0.001* |
| >10–20 years (n = 375) | 60                        | 0.63  | 1.88 (1.30–2.71)   | 0.001*  |
| >20–30 (n = 551)       | 64                        | 0.26  | 1.29 (0.91–1.85)   | 0.150   |
| >30–40 (n = 416)       | 37                        | −0.04 | 0.96 (0.64–1.46)   | 0.863   |
| >40 years (n = 794)    | 73                        |       | Reference category |         |

n = sample number.  
\*Statistically significant.

were found for children ≤5 years and >5–10 years ( $P < 0.001$ ) (Table 2). An age-dependent infection status was also apparent with the two major coinfecting pathogens, *V. cholerae* in the ≤5-year ( $P < 0.001$ ) and rotavirus in >5–10-year ( $P < 0.001$ ) group. Interestingly, coinfections of *Giardia* and other diarrheal-causing pathogens showed a marked decline with increasing age compared with infections with *Giardia* alone (Figure 4(a)).

In spite of observing a trend in the monthly isolation rate for *G. duodenalis*, no seasonality pattern could be inferred from the data; this may be because isolation of the parasite is dependent on the total number of diarrheal cases and this

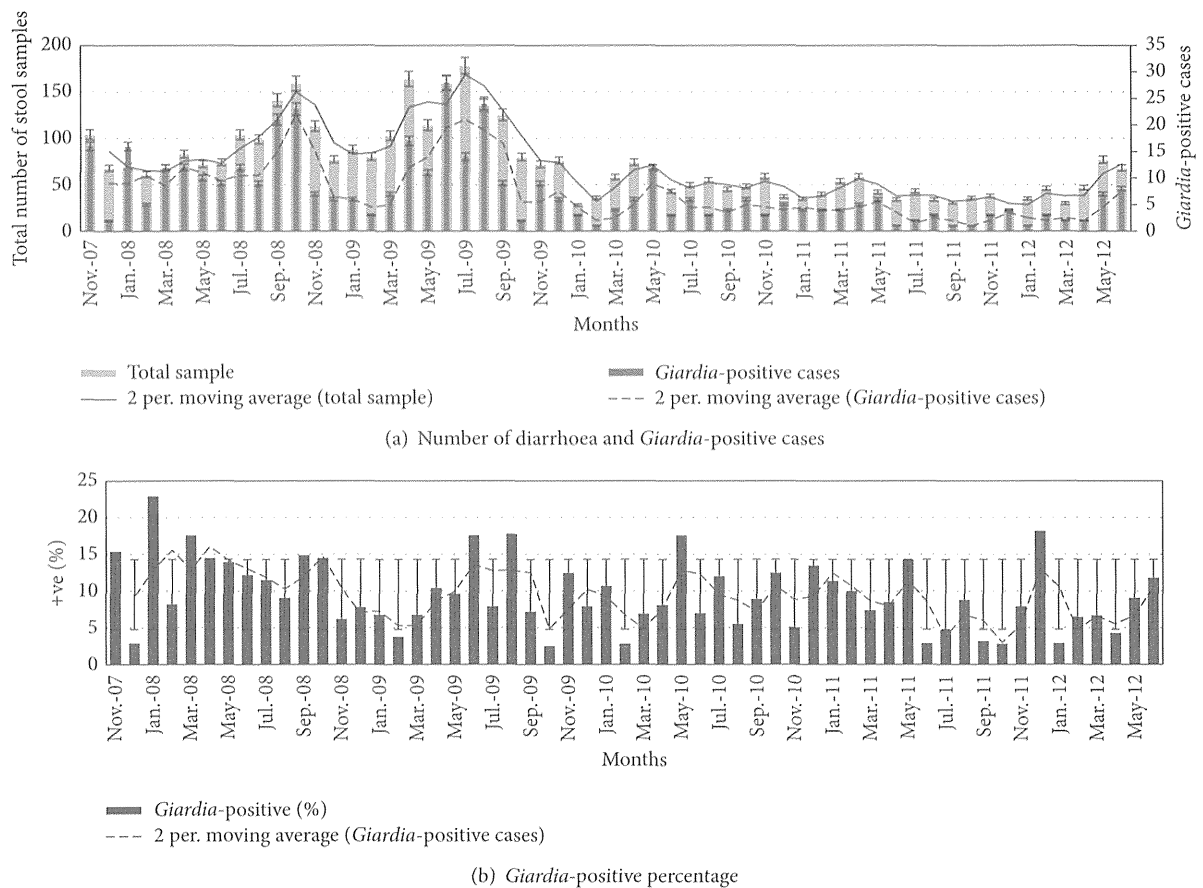


FIGURE 2: Month-wise distribution of diarrhoeal cases and *Giardia*-positive cases. (a) The total number of stool samples tested per month throughout the study period and the number of *Giardia*-positive cases recorded for the same period. Note that different y-axis scales have been used for clarity. Trend lines representing the sample distribution and *Giardia*-positive cases are similar. (b) Percentage of *Giardia*-positive cases each month. The data show constant deviation and a nonexplanatory trend line.

number changes according to the season. However, the steady rates of infection seen in the dry seasons could indicate that *G. duodenalis* is not dependent on rainfall. In this regard, the finding that *Giardia* infections were strongly associated with coinfection ( $P \leq 0.001$ ) suggests that the parasite derives some advantage from the presence of other diarrhoea-causing pathogens in the host, or vice versa. Similarly, *G. duodenalis* was found to be most prevalent in  $\leq 5$ -year and  $> 5$ -10-year olds, suggesting that age can be a determining factor for increased susceptibility to Giardiasis. Interestingly, in both of these age groups, coinfections of *Giardia* and rotavirus in children  $\leq 5$  years and *Vibrio cholerae* in children above 5-10 years were common (Figure 4(b)). As with previous studies, infection with *V. cholerae* or rotavirus is common in the lower age groups [18] in the study region. This suggests that *Giardia* could in some way take benefit from the major pathogens prevalent in a particular population at a particular time. This could explain the lack of seasonality and steady infection rates among diarrhoeal cases in regions where *Giardia* is endemic. In the present study, the *G. duodenalis* infection rate is high in the monsoon or postmonsoon period, as did *V. cholerae* and other bacterial pathogens that are associated with water contamination from uncontrolled sewage dispersal in the

rainy seasons. However, the rate is also high in the winter, along with coinfecting pathogens such as rotavirus.

#### 4. Conclusions

The high rate of *Giardia* infection seen throughout the study period across all climatic conditions and the significant association of *Giardia* with other major pathogens suggest that the parasite may play a role in regulating the spectrum of diarrhoeal disease in the study area. A statistically significant association with *Vibrio cholerae* and rotavirus across two different seasons suggests that *Giardia* may have evolved to survive in the diarrhoea-prone endemic region investigated herein. The opportunistic nature of *Giardia* is previously considered as an opportunistic pathogen so it can be a major reason for the observation. Otherwise, the coinfection status could be a reason for coexistence of *Giardia* and other pathogens in the infection source, that is, food and water. *Giardia* appears to be maintaining the characteristics of an ideal opportunistic pathogen, resulting in a steady but high prevalence rate in a population and eventually making the population more susceptible to other major diarrhoeal infections.

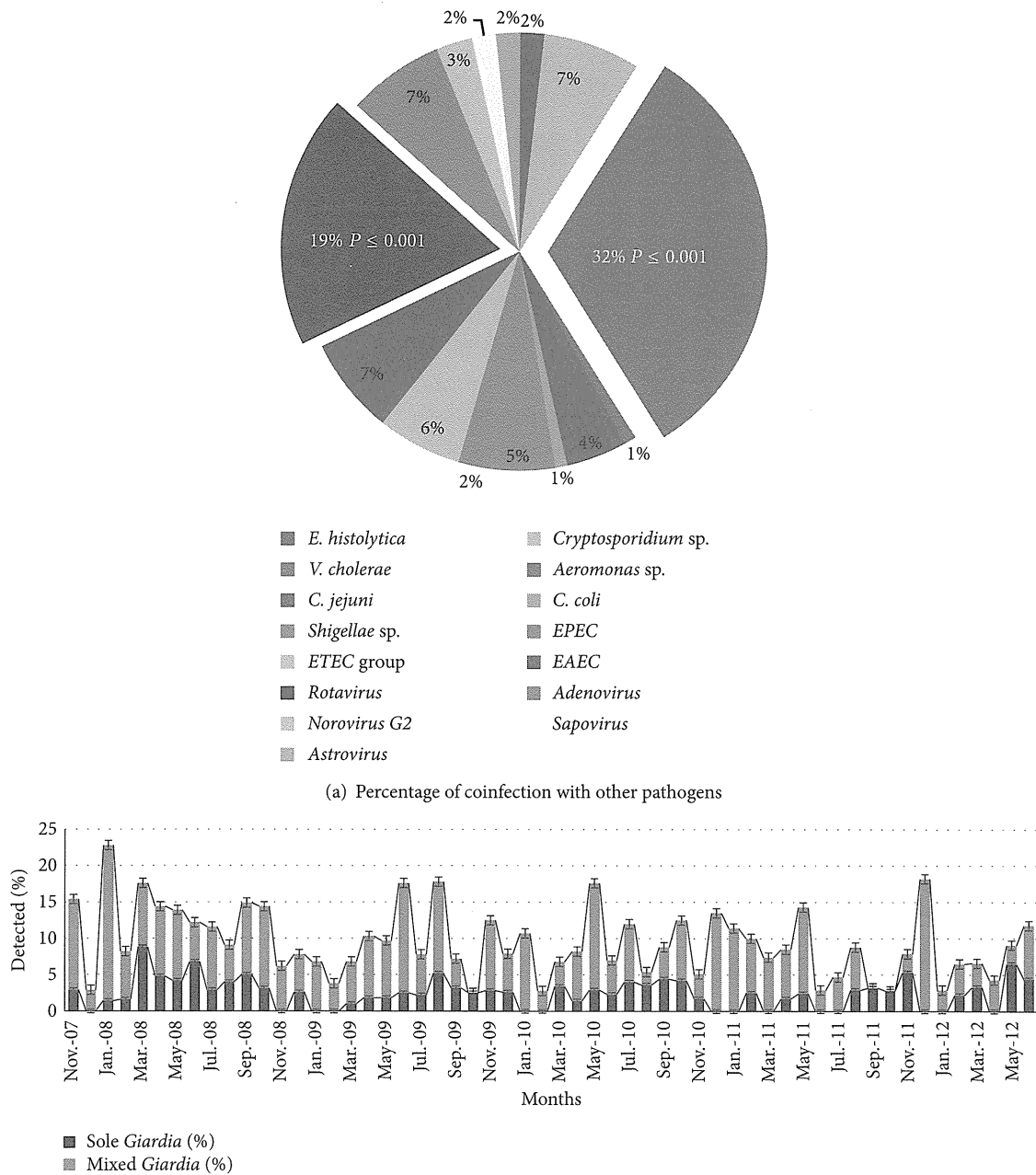


FIGURE 3: Coinfection of *Giardia duodenalis* with other enteric pathogens. (a) Coinfection of *Giardia* with other pathogens. *Vibrio cholerae* and rotavirus rates are highest and have statistically significant associations ( $<0.001$ ) with the total number of *Giardia* cases. (b) Monthly prevalence of single and mixed *Giardia duodenalis* infections throughout the study period.

**Abbreviations**

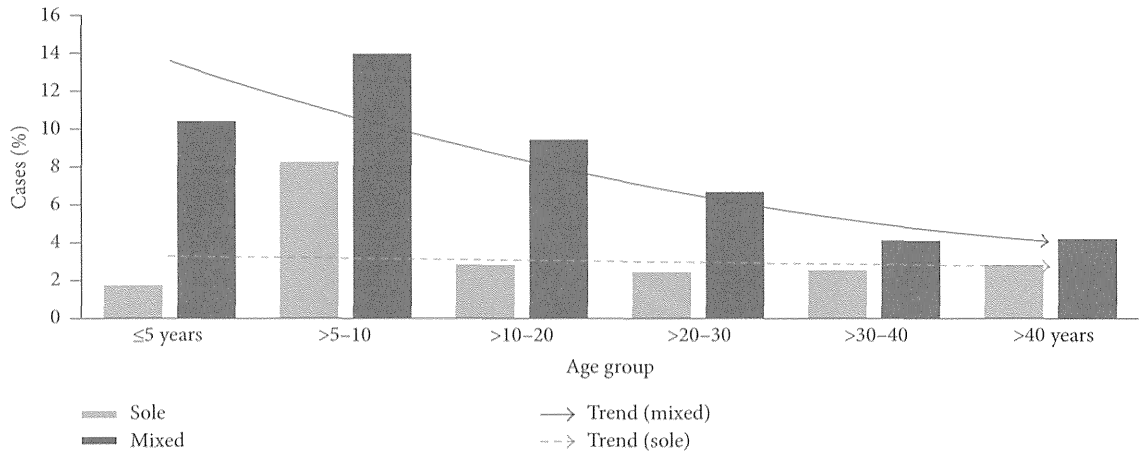
IDBG: Infectious Diseases and Beliaghata General  
 NICED: National Institute of Cholera and Enteric Diseases  
 DALY: Disability Adjusted Life Year.

**Conflict of Interests**

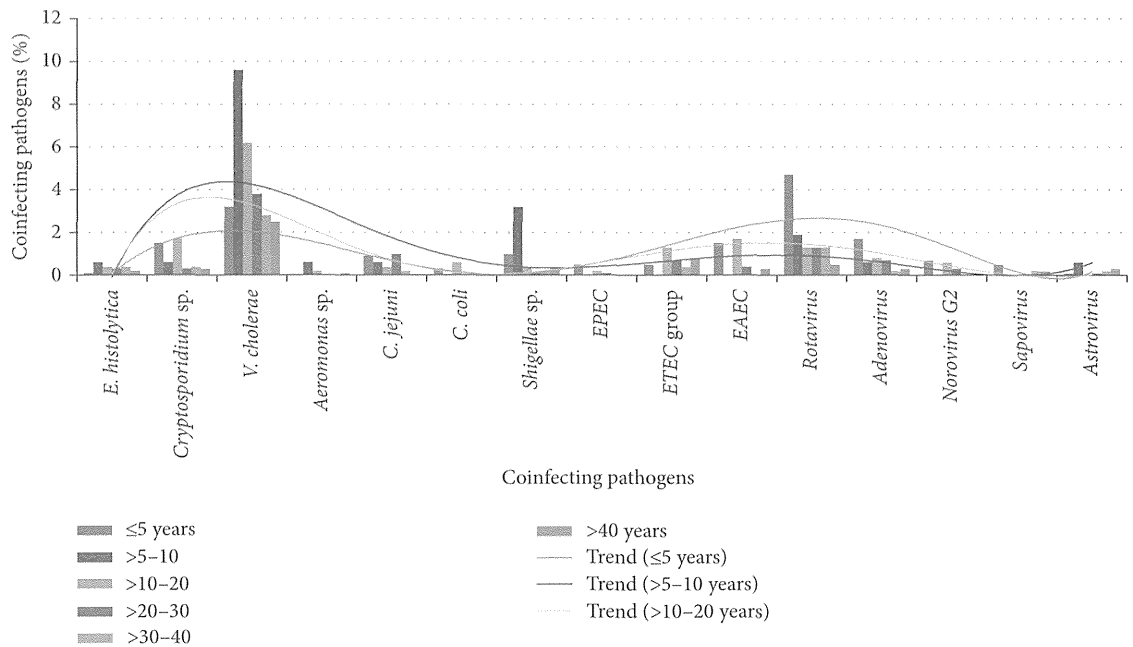
The authors declare no conflict of interests for this particular study.

**Authors' Contribution**

Avik K. Mukherjee contributed to data acquisition and analysis, conceived the study, and wrote the draft paper. Punam Chowdhury helped with pathogen detection and laboratory data storage. Krishnan Rajendran performed the statistical analysis and data management. omoyoshi Nozaki helped in addressing reviewer's comments and doing critical review of the manuscript. Sandipan Ganguly performed the



(a) Age distribution of sole and mixed *Giardia* infection



(b) Coinfection status of *G. duodenalis* stratified by age group

FIGURE 4: Age-wise distribution of *Giardia* and its relationship with coinfecting pathogens. (a) Distribution of single infections of *Giardia* and mixed infections with other pathogens across six age categories. Note the decreasing slope of the trend line in the older age groups. (b) Age distribution of *Giardia* cases according to their coinfection status with other pathogens. Trend line of  $\leq 5$  years shows that coinfection is highest for rotavirus, followed by *Vibrio cholerae*, and for the  $>5-10$  and  $>10-20$  age groups coinfection with *V. cholerae* is higher.

final analysis, evaluated all of the results, checked the paper, and gave final approval for paper publication.

**Acknowledgments**

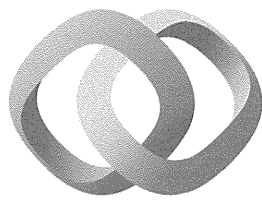
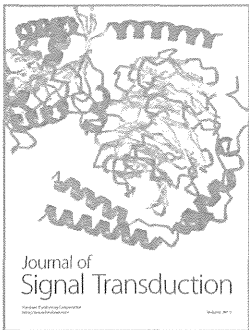
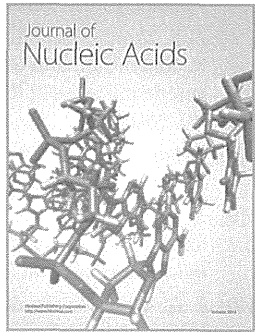
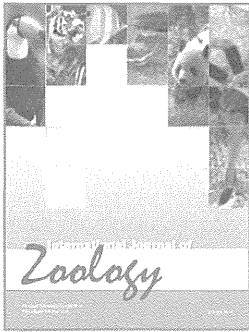
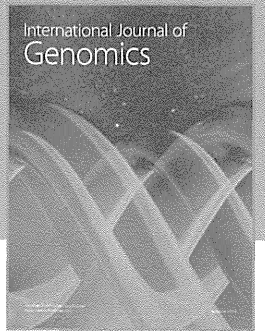
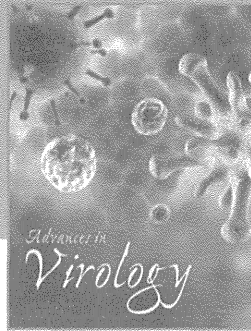
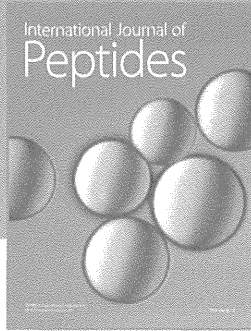
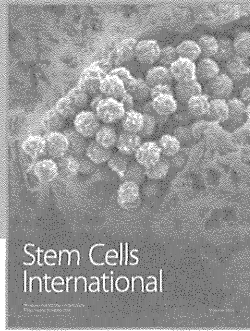
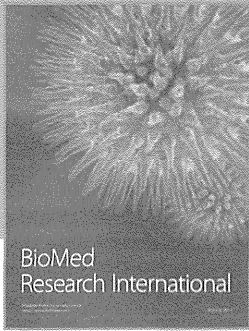
This study was jointly supported by a grant from the Okayama University Program of Founding Research Centre for Emerging and Reemerging Infectious Disease, Ministry of Education, Culture, Sports, Science and Technology of Japan, and the Japan Health and Science Foundation, Government of Japan, National Institute of Infectious Diseases, Tokyo, Japan and Indian Council of Medical Research, Government

of India. The authors thank all of the patients and field workers who participated in the study. They also thank Dr. Mrinmoy Ghosh for arranging the stool sample collections at IDBG hospital.

**References**

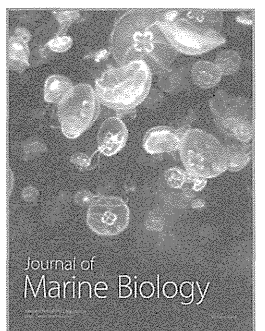
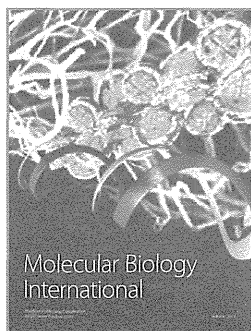
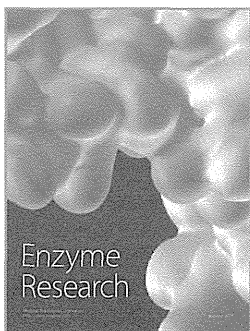
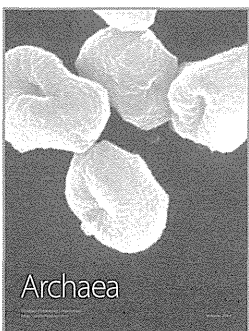
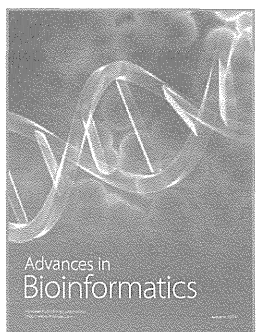
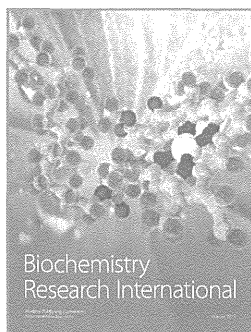
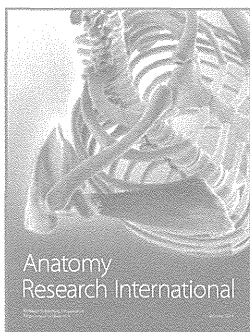
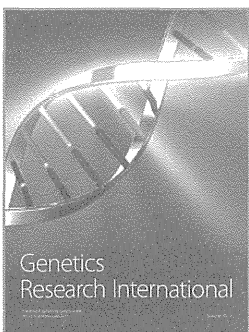
[1] G. G. Fraser and K. R. Cooke, "Endemic giardiasis and municipal water supply," *American Journal of Public Health*, vol. 81, no. 6, pp. 760-762, 1991.  
 [2] A. Odoi, S. W. Martin, P. Michel, J. Holt, D. Middleton, and J. Wilson, "Determinants of the geographical distribution of endemic giardiasis in Ontario, Canada: a spatial modelling

- approach," *Epidemiology and Infection*, vol. 132, no. 5, pp. 967–976, 2004.
- [3] R. D. Adam, "The *Giardia lamblia* genome," *International Journal for Parasitology*, vol. 30, no. 4, pp. 475–484, 2000.
- [4] GBD, *Summary Tables*, Health Statistics and Informatics Department, World Health Organization, Geneva, Switzerland, 2004, <http://www.who.int/evidence/bod>.
- [5] D. B. Huang and A. C. White, "An updated review on *Cryptosporidium* and *Giardia*," *Gastroenterology Clinics of North America*, vol. 35, no. 2, pp. 291–314, 2006.
- [6] G. B. Nair, T. Ramamurthy, M. K. Bhattacharya et al., "Emerging trends in the etiology of enteric pathogens as evidenced from an active surveillance of hospitalized diarrhoeal patients in Kolkata, India," *Gut Pathogens*, vol. 2, no. 1, article 4, 2010.
- [7] A. K. Mukherjee, P. Chowdhury, M. K. Bhattacharya, M. Ghosh, K. Rajendran, and S. Ganguly, "Hospital-based surveillance of enteric parasites in Kolkata," *BMC Research Notes*, vol. 2, article 110, 2009.
- [8] "Diagnostic procedures for stool specimens," <http://www.dpd.cdc.gov/dpdx/HTML/DiagnosticProcedures.htm>.
- [9] A. V. Allen and D. S. Ridley, "Further observations on the formol-ether concentration technique for faecal parasites," *Journal of Clinical Pathology*, vol. 23, no. 6, pp. 545–546, 1970.
- [10] P. A. Rochelle, R. de Leon, M. H. Stewart, and R. L. Wolfe, "Comparison of primers and optimization of PCR conditions for detection of *Cryptosporidium parvum* and *Giardia lamblia* in water," *Applied and Environmental Microbiology*, vol. 63, no. 1, pp. 106–114, 1997.
- [11] A. G. Dean, T. G. Arner, G. G. Sunki et al., *Epi Info, A Database and Statistics Program for Public Health Professionals*, Centers for Disease Control and Prevention, Atlanta, Ga, USA, 2011.
- [12] S. Menard, "Coefficients of determination for multiple logistic regression analysis," *The American Statistician*, vol. 54, no. 1, pp. 17–24, 2000.
- [13] D. W. Hosmer Jr. and S. Lemeshow, *Applied Logistic Regression*, John Wiley & Sons, New York, NY, USA, 2nd edition, 2000.
- [14] S. N. Goodman, "Toward evidence-based medical statistics. 1: the P value fallacy," *Annals of Internal Medicine*, vol. 130, no. 12, pp. 995–1004, 1999.
- [15] R. R. Frerichs, "History, maps and the internet: UCLA's John Snow site," *Bulletin of the Society of Cartographers*, vol. 34, no. 2, pp. 3–7, 2000.
- [16] J. Plutzer, A. Törökné, Z. Szénási, I. Kucsera, K. Farkas, and P. Karanis, "Detection and genotype analysis of *Giardia duodenalis* from asymptomatic Hungarian inhabitants and comparative findings in three distinct locations," *Acta Microbiologica et Immunologica Hungarica*, vol. 61, no. 1, pp. 19–26, 2014.
- [17] M. Ish-Horowicz, S. H. Korman, M. Shapiro et al., "Asymptomatic giardiasis in children," *Pediatric Infectious Disease Journal*, vol. 8, no. 11, pp. 773–779, 1989.
- [18] K. Rajendran, A. Sumi, M. K. Bhattachariya et al., "Influence of relative humidity in *Vibrio cholerae* infection: a time series model," *Indian Journal of Medical Research*, vol. 133, no. 2, pp. 138–145, 2011.



Hindawi

Submit your manuscripts at  
<http://www.hindawi.com>





# Interaction between Nbp35 and Cfd1 Proteins of Cytosolic Fe-S Cluster Assembly Reveals a Stable Complex Formation in *Entamoeba histolytica*

Shadab Anwar<sup>1</sup>, Manas Ranjan Dikhit<sup>2</sup>, Krishn Pratap Singh<sup>1</sup>, Rajiv Kumar Kar<sup>2</sup>, Amir Zaidi<sup>1</sup>, Ganesh Chandra Sahoo<sup>2</sup>, Awadh Kishore Roy<sup>3</sup>, Tomoyoshi Nozaki<sup>4</sup>, Pradeep Das<sup>5</sup>, Vahab Ali<sup>1\*</sup>

**1** Laboratory of Molecular Biochemistry and Cell Biology, Department of Biochemistry, Rajendra Memorial Research Institute of Medical Sciences, Agam-kuan, Patna, India, **2** Department of Biomedical Informatics Centre, Rajendra Memorial Research Institute of Medical Sciences, Agam-kuan, Patna, India, **3** Department of Botany, T. M. Bhagalpur University, Bhagalpur, India, **4** Department of Parasitology, National Institute of Infectious Diseases, Shinjuku-ku, Tokyo, Japan, **5** Department of Molecular Biology, Rajendra Memorial Research Institute of Medical Sciences, Agam-kuan, Patna, India

## Abstract

Iron-Sulfur (Fe-S) proteins are involved in many biological functions such as electron transport, photosynthesis, regulation of gene expression and enzymatic activities. Biosynthesis and transfer of Fe-S clusters depend on Fe-S clusters assembly processes such as ISC, SUF, NIF, and CIA systems. Unlike other eukaryotes which possess ISC and CIA systems, amitochondriate *Entamoeba histolytica* has retained NIF & CIA systems for Fe-S cluster assembly in the cytosol. In the present study, we have elucidated interaction between two proteins of *E. histolytica* CIA system, Cytosolic Fe-S cluster deficient 1 (Cfd1) protein and Nucleotide binding protein 35 (Nbp35). *In-silico* analysis showed that structural regions ranging from amino acid residues (P33-K35, G131-V135 and I147-E151) of Nbp35 and (G5-V6, M34-D39 and G46-A52) of Cfd1 are involved in the formation of protein-protein complex. Furthermore, Molecular dynamic (MD) simulations study suggested that hydrophobic forces surpass over hydrophilic forces between Nbp35 and Cfd1 and Van-der-Waal interaction plays crucial role in the formation of stable complex. Both proteins were separately cloned, expressed as recombinant fusion proteins in *E. coli* and purified to homogeneity by affinity column chromatography. Physical interaction between Nbp35 and Cfd1 proteins was confirmed *in vitro* by co-purification of recombinant Nbp35 with thrombin digested Cfd1 and *in vivo* by pull down assay and immunoprecipitation. The *insilico, in vitro* as well as *in vivo* results prove a stable interaction between these two proteins, supporting the possibility of its involvement in Fe-S cluster transfer to target apo-proteins through CIA machinery in *E. histolytica*. Our study indicates that initial synthesis of a Fe-S precursor in mitochondria is not necessary for the formation of Cfd1-Nbp35 complex. Thus, Cfd1 and Nbp35 with the help of cytosolic NifS and NifU proteins can participate in the maturation of non-mitosomal Fe-S proteins without any apparent assistance of mitochondria.

**Citation:** Anwar S, Dikhit MR, Singh KP, Kar RK, Zaidi A, et al. (2014) Interaction between Nbp35 and Cfd1 Proteins of Cytosolic Fe-S Cluster Assembly Reveals a Stable Complex Formation in *Entamoeba histolytica*. PLoS ONE 9(10): e108971. doi:10.1371/journal.pone.0108971

**Editor:** Tracey Rouault, National Institute of Child Health and Human Development, United States of America

**Received:** March 8, 2014; **Accepted:** August 29, 2014; **Published:** October 1, 2014

**Copyright:** © 2014 Anwar et al. This is an open-access article distributed under the terms of the Creative Commons Attribution License, which permits unrestricted use, distribution, and reproduction in any medium, provided the original author and source are credited.

**Data Availability:** The authors confirm that all data underlying the findings are fully available without restriction. All data are included within the paper.

**Funding:** This work was supported by a grant from Indian Council of Medical Research (ICMR), Ministry of Health and Family Welfare, and Department of Science & Technology (DST/INT/JSPSP-117), New Delhi, India. The funder had no role in study design, data collection and analysis decision to publish, or preparation of the manuscript.

**Competing Interests:** The authors have declared that no competing interests exist.

\* Email: vahab\_ali@yahoo.com

## Introduction

*Entamoeba histolytica* is one of the most widespread and clinically important protozoan parasite causing both intestinal (amoebic colitis) and extra intestinal (amoebic liver abscess) disease throughout the world, resulting to an estimated 40,000 to 110,000 deaths annually. World Health Organisation estimate (WHO, 1998) places *E. histolytica* second after *Plasmodium falciparum* in causing abundant annual death among protozoan parasites. *E. histolytica* lacks a defined structure of mitochondria and its functions [1]. However, mitochondrion residual organelle known as mitosome [2] is present in this parasite. Mitochondria performs many crucial roles in various biochemical and iron-requiring biosynthetic processes; namely, heme formation, Iron-Sulfur (Fe-S) clusters biogenesis and cellular iron regulation [3,4]. Among them, Iron-Sulfur clusters biogenesis is essential for the maturation of Fe-

S proteins which are biologically functional and ubiquitous components that orchestrate a wide range of biochemical machinery and efficiently regulate the metabolic cascades in living organisms for sustainable and fundamental life processes [4–8]. Mitochondria assemble Fe-S clusters for their own set of mitochondrial Fe-S proteins as well as crucially involved in the biogenesis and maturation of Fe-S proteins located in the cytosol and nucleus [9–11].

Despite the chemical simplicity of Fe-S clusters, Fe-S clusters biogenesis is a complex process involving three types of systems, viz, Iron Sulfur Clusters (ISC), Sulfur Utilization Factors (SUF) and Nitrogen Fixation (NIF) systems. The ISC system is a house-keeping system involving ~30 protein components [8,12–14] and among them 10 proteins have been conserved from bacteria to human [15,16]. The majority of protozoan parasites have retained



ISC system either in mitochondrion or mitochondria like organelles; mitosomes, hydrogenosomes, and mitochondria related organelles (MROs) [17–20]. However, *Plasmodium spp.* & *Blastocystis hominis* possess SUF system or some of its components in addition to the canonical ISC system which is functional under oxidative stress and iron deficient conditions [19,21–23]. Nitrogen-fixation (NIF) system is present in nitrogen fixing bacteria, cyanobacteria and microaerophilic bacteria but absent in eukaryotes and protozoan parasites except *E. histolytica* and free living amoeba (*Mastigamoeba balamuthi*). Thus, Fe-S cluster biogenesis in *E. histolytica* solely depends on NIF system [24]. It has already been proved that the NIF system alone is required for the biosynthesis of Fe-S cluster in *E. histolytica* under anaerobic conditions [24]. This organism possesses two components of NIF machinery: NifS and NifU [24,25] that are responsible for Fe-S cluster assembly. Surprisingly, *M. balamuthi* possesses two types of NifS and NifU components, of which one of them has retained targeting signal and localized in the mitosomes [26]. Contrary to the mitosomes of *M. balamuthi*, *E. histolytica* mitosomes have no evidence of classic Fe-S cluster machinery. Therefore, cytosolic NIF machinery predominantly regulates the cellular requirements for Fe-S cluster biogenesis in this organism. *E. histolytica* possess mitosomes that do not generate ATP unlike other protozoan parasites harbouring MROs (*Blastocystis sp.*) or hydrogenosomes which are involved in both ATP generation and Fe-S cluster biogenesis [27]. However, neither amoebic mitosomes possesses the ISC machinery, nor any component of ISC or SUF machinery has been identified in *E. histolytica* genome [23]. It has not been resolved till-date how NIF system works in connection with Cytosolic Iron-sulfur protein Assembly (CIA) in the absence of true mitochondria. It also remains unknown whether NIF and CIA system interact with each other for biogenesis and subsequent transfer of Fe-S clusters to apoproteins, as both systems co-exist in the cytoplasm.

In eukaryotes, the ISC system assists for the maturation of cytosolic/nuclear Fe-S proteins including CIA machinery components. The CIA system is limited to cytoplasm and core protein assembly consists of Cfd1, Nbp35, Nar1, Cia1, Dre2, Tah18 [28–34] and some additional components (MMS19, MIP18 and ANT2) which are exclusively present in mammalian system [35]. MMS19 function as part of the CIA machinery which interacts and facilitate Fe-S cluster targeting to apo-proteins involved in methionine biosynthesis, DNA replication, DNA repair, and telomerase maintenance [36]. In addition, MMS19 forms a complex with CIA proteins (CIAO1, IOP1, & MIP18) involved in DNA metabolism and its presence is necessary for DNA replication and repair [37]. The CIA1 (CIAO1) associates with either CIA2A (FAM96A) or CIA2B (FAM96B) and MMS19 proteins. It has been reported recently that CIA2B-CIA1-MMS19 complex binds to and facilitates assembly of most cytosolic/nuclear Fe-S proteins but CIA2A is specially required for the maturation of iron regulatory protein 1 (IRP1), which is involved in cellular iron homeostasis [38]. The CIA2A is also involved in stabilization of IRP2 through its interaction with IRP2. However, *E. histolytica*, comprised of a NIF system has also retained CIA components namely; Cfd1, Nbp35, Nar1, Dre2, and Cia1 [23]. Cfd1 and Nbp35 belong to a subfamily of deviant P-loop NTPases, often referred to as the MRP/NBP35 sub-family, which appear to function in Fe-S clusters biogenesis in all kingdoms. The first component of the CIA machinery to be identified was Cfd1 which is an essential and highly conserved P-loop NTPase [29]. *In vitro* reconstitution study has shown that Nbp35 forms an oligomeric complex with Cfd1 and both can assemble labile Fe-S cluster on their conserved cysteine residues of C-terminal domain. They may serve as transient scaffold for Fe-S cluster before transfer to apo-proteins in yeast [39,40]. The class of NTPases typically form homodimer involving a signature lysine (Lys26 in Cfd1 and Lys81 in Nbp35) residue within the walker A (Nucleotide binding) motif which also plays a role in ATP binding

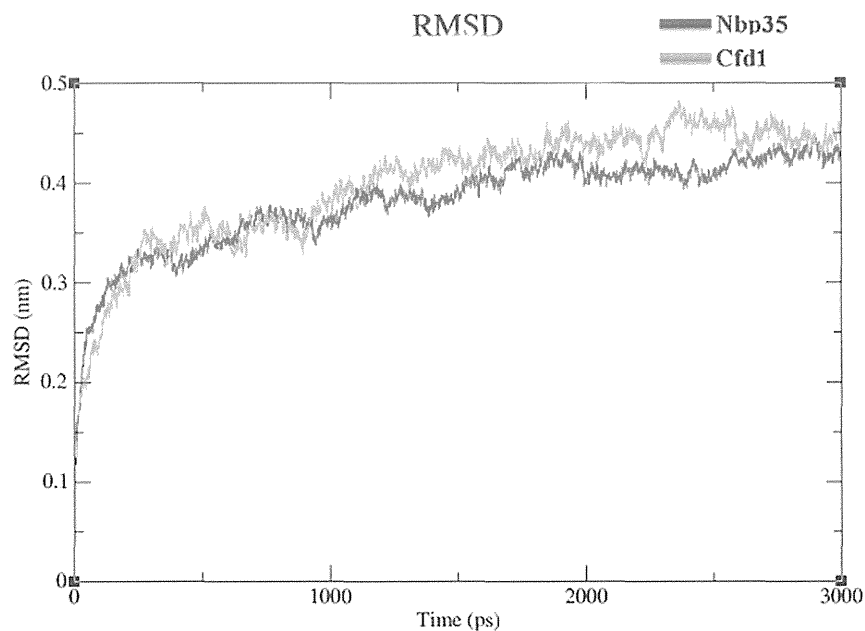


**Figure 1. RMSDs time scan for Nbp35 and Cfd1.** Backbone RMSDs are shown as a function of time for Nbp35 (red) and Cfd1 (green) protein at 3 ns.

doi:10.1371/journal.pone.0108971.g001



and/or hydrolysis [41]. However, in plantae including *Arabidopsis thaliana*, Cfd1 is absent and Npb35 works alone as the scaffold component [42,43]. Although, Cfd1 gene is absent in some organisms such as *Caenorhabditis elegans* (metazoa) and plantae [43]; the specific functional role of Cfd1 is its interaction with Nbp35 which alters the character of Nbp35-bound Fe-S clusters, making it more labile and enhancing transfer to apo-target Fe-S proteins [41].

In the present study, we have attempted to investigate the interaction between Cfd1 and Nbp35 in *E. histolytica in vivo* by co-purification and immunoprecipitation and *insilico* using molecular dynamics simulation tool. Our results show that Npb35 and Cfd1 of *E. histolytica* interacts with each other to form a stable complex and each protein has the potential to coordinate a 4Fe-4S cluster on it similar to the earlier report in yeast [30,40]. This would be the first report showing interaction and stable complex formation between two components of CIA machinery Nbp35 and Cfd1 in an amitochondriate protozoan parasite possessing a cytosolic NIF system for Fe-S cluster assembly.

## Materials and Methods

### Chemicals and reagents

All chemicals of analytical grade were purchased and used from Sigma-Aldrich, Amresco (USA), Merck, and USB (USA) unless otherwise stated. Chromatography column was purchased from Bio-Rad. Ni<sup>2+</sup>-NTA agarose was purchased from Qiagen. Adult bovine serum from Hyclone, Yeast extract and Casitone were purchased from BD Biosciences.

### Microorganism and cultivation

*E. histolytica* trophozoites clonal strain (HM-1: IMMS cl 6) was maintained axenically in TYIS-33 medium supplemented with 15% adult bovine serum at 35.5°C [44]. Trophozoites were harvested in the late-logarithmic growth phase 2–3 days after the inoculation of medium with one-thirtieth to one-twelfth of the total culture volume. After the cultures were chilled on ice for 5 mins, trophozoites were collected by centrifugation at 500×g for 10 mins at 4°C and washed twice with ice-cold phosphate-

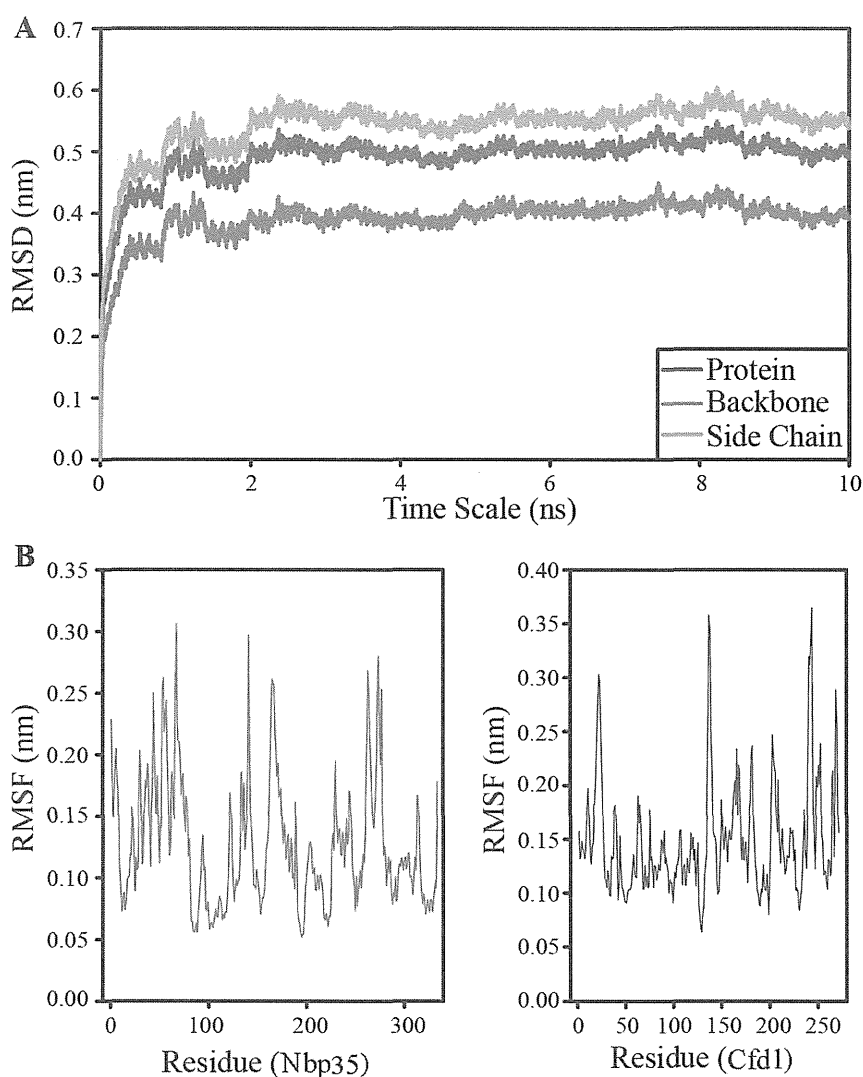


**Figure 2. RMSD and RMSF profile of Nbp35-Cfd1 complex.** (A) RMSD profile of Nbp35-Cfd1 complex for all-atoms (red), backbone atoms (blue) and side chain (green) plotted as a function of time (B) Root mean square fluctuation for Nbp35 and Cfd1 plotted against time from MD simulation.

doi:10.1371/journal.pone.0108971.g002

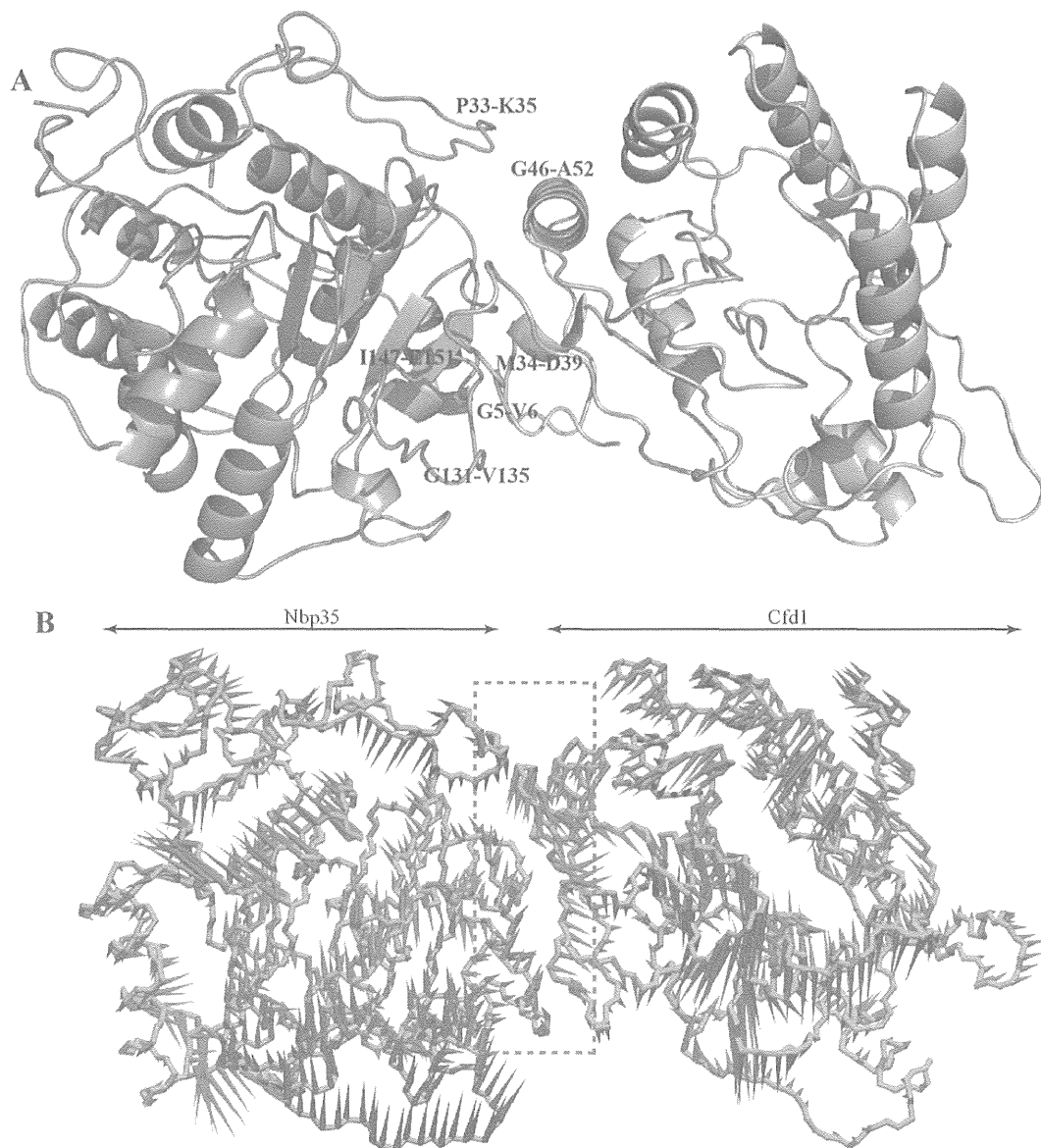


**Figure 3. Nbp35-Cfd1 complex structure showing the regions involved in interaction.** (A) Complex structure of Nbp35-Cfd1 where the molecular contacts are highlighted (blue-Nbp35) and (green-Cfd1) with mentioned residues involved in interaction. (B) Porcupine plots for Nbp35-Cfd1 complex showing backbone fluctuation from simulation time course. The regions involved in contact are highlighted with dotted region. doi:10.1371/journal.pone.0108971.g003

buffered saline (PBS), pH 7.4 [45]. Cell pellets were stored at  $-30^{\circ}\text{C}$  until use.

#### PCR amplification and cloning of Nbp35 & Cfd1 genes

Based on the nucleotide sequence of the protein-encoding region of the putative *E. histolytica* Nucleotide binding proteins genes (*Nbp35*, accession number XP\_650593, EHI\_047750; *Cfd1* accession number XP\_653192; EHI\_000610); primers (shown below) were designed to clone Nbp35 & Cfd1 in vector pET15b with a histidine tag at the amino terminus. The *Nbp35* & *Cfd1* ORFs were amplified from cDNA of *E. histolytica* with a sense (5'-CCTCATATGAGTTGTTCTCATAATTGTTCA-3') and an antisense (5'-CCAGGATCC**TTAA**GATTTGTTATTATTTCCIT-3') primers for Nbp35 and a sense (5'-CCTCATATGACTGAAC**TTAA**CTCTGATCGT-3') and an antisense (5'-CCAGGATCC**TTAA**GCAAAAAGTTT**TAGCA**AGATCG-3') primers

for Cfd1, where *NdeI* and *BamHI*-sites are underlined and the translation initiation and termination codons are italicized. PCR was performed in a 50  $\mu\text{l}$  volume containing 0.25 mM each dNTPs, 2.0 mM  $\text{MgCl}_2$ , 1.0  $\mu\text{M}$  each primer, 1  $\mu\text{g}$  cDNA (*E. histolytica*) and 1.0 U Pfu DNA polymerase. The conditions used to amplify the *Nbp35* & *Cfd1* genes were hot start at  $94^{\circ}\text{C}$  for 5 mins, denaturation at  $94^{\circ}\text{C}$  for 30 s, annealing at  $55^{\circ}\text{C}$  for 30 s, elongation at  $68^{\circ}\text{C}$  for 1.0 min and subjected to 30 cycles with a final extension for 10 mins at  $68^{\circ}\text{C}$ . A  $\sim 1.0$  & 0.8 kb PCR products were observed on 1.0% agarose gel electrophoresis. These PCR products were double digested with *NdeI* and *BamHI*, electrophoresed, purified with gel extraction kit (Qiagen), and cloned into *NdeI* and *BamHI*-digested pET-15b (Novagen) in the same orientation as the T7 promoter. The ligated mixture was transformed in competent DH5 $\alpha$  cells (Novagen) which produced the pET-15b-Nbp35 & pET-15b-Cfd1 plasmids. The insert and

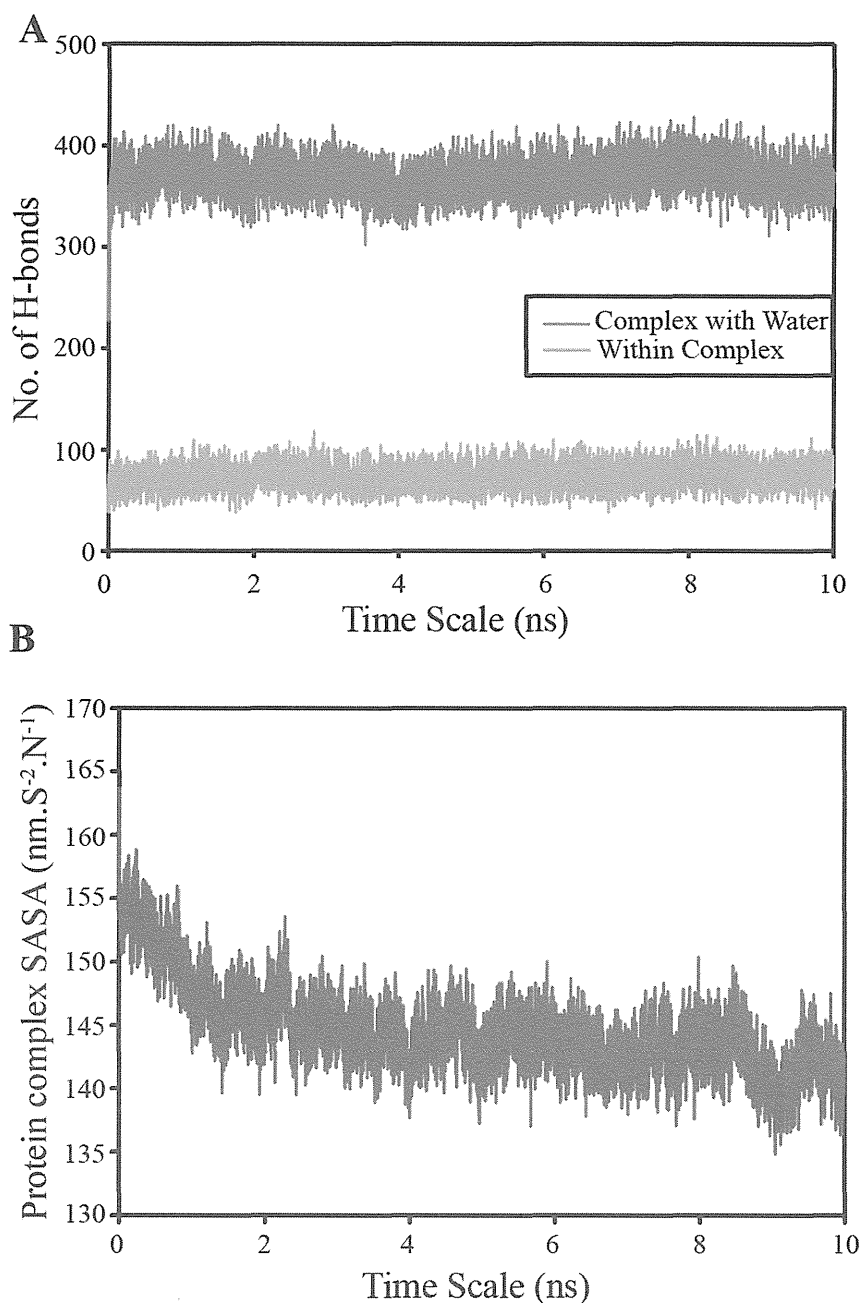


**Figure 4. Hydrogen bonding profile & solvent accessibility.** (A) Hydrogen bonding profile indicating numbers of hydrogen bonds formed within protein atoms and with water molecules. (B) Solvent accessible surface area computed over the simulation time course.  
doi:10.1371/journal.pone.0108971.g004

ORF orientation were confirmed by colony PCR. Construct plasmids were isolated using Qiagen miniprep kit as per manufacturer's instructions. The pET-15b-Nbp35 & pET-15b-Cfd1 constructs were transformed into competent *E. coli* BL21 (DE3) (Novagen) cells by heat shock at 42°C for 45 s, and the cells were grown at 37°C on Luria Bertani (LB) agar medium in the presence of 50 µg/ml ampicillin (Amp).

#### Expression and purification of recombinant Nbp35 and Cfd1 Proteins

The pET-Nbp35 and pET-Cfd1 expression constructs were introduced into competent cells and the resulting single colony

picked up from LB-agar plate were grown at 37°C in 5 ml of LB medium in the presence of 50 µg/ml ampicillin. The overnight culture was used to inoculate 500 ml of fresh medium and cultured at 37°C with shaking at 200 rpm. When the  $A_{600}$  reached 0.6, 0.4 mM of isopropyl β-D- thiogalactopyranoside was added to induce protein expression for 12 h at 25°C. *E. coli* cells were harvested by centrifugation at 5000 rpm for 10 mins at 4°C, the resulting cell pellet washed with PBS (pH 7.4) and resuspended in 25 ml lysis buffer [46] containing 100 µg/ml lysozyme and 1 mM Phenylmethylsulfonyl fluoride (PMSF). After 45 mins of incubation at 30°C, the cells were sonicated on ice and centrifuged at 13000 rpm for 20 mins at 4°C. The supernatant was mixed with

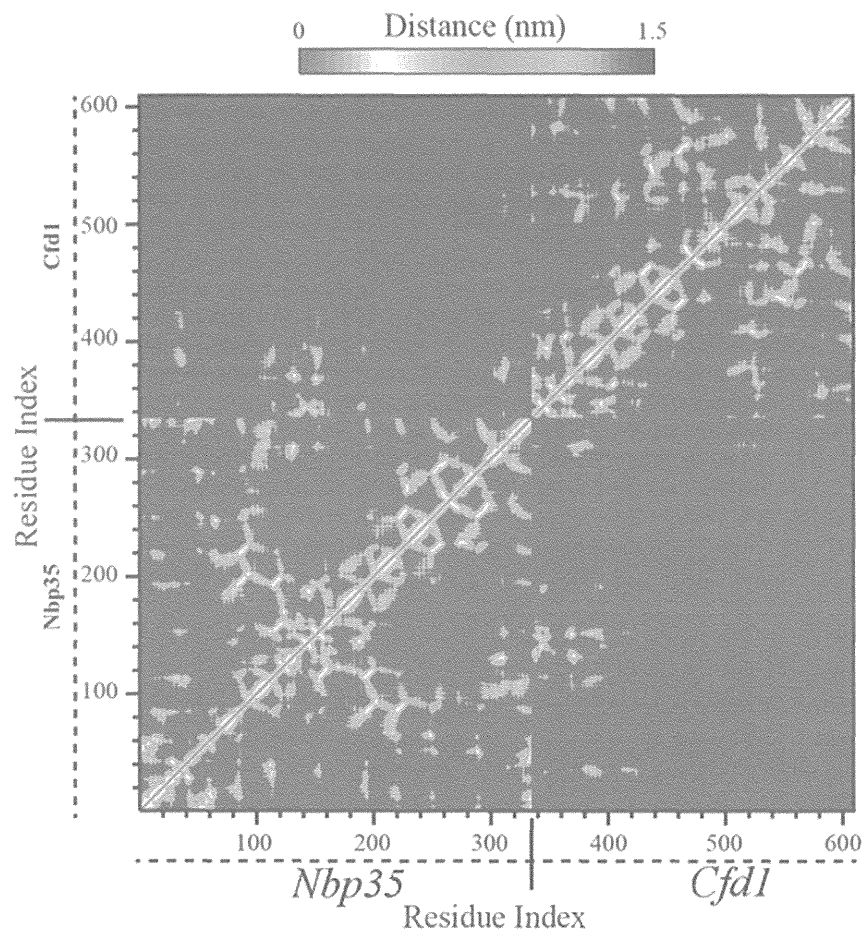


**Figure 5. Contact map of Nbp35-Cfd1 complex.** The contact map of Nbp35-Cfd1 complex is indicating the cross residue region involved in contact of these two proteins.  
doi:10.1371/journal.pone.0108971.g005

500  $\mu$ l of Ni<sup>2+</sup>-NTA His-tag slurry (Qiagen) and incubated for 1.0 hr at 4°C with gentle shaking. The recombinant Nbp35 and Cfd1 protein bound resin was washed with 8–10 column volumes of buffer A (50 mM Tris-HCl, pH 8.0, 300 mM NaCl, and 0.1% Triton X-100, v/v) containing 10–50 mM of imidazole and bound proteins were eluted in 2–3 ml with buffer A containing 100–300 mM imidazole. The quality and purity of the rNbp35 and rCfd1 proteins were confirmed by 12% SDS-PAGE analysis. The proteins were extensively dialyzed against a 300 fold volume of 50 mM Tris-HCl, 150 mM NaCl, pH 8.0, containing 10% glycerol (V/V) and the complete Mini protease inhibitor cocktail (Calbiochem). The concentration of the dialyzed proteins was determined by Bradford method using bovine serum albumin as standard (U3900, Hitachi, Japan). The rNbp35 and rCfd1 proteins were stored at –30°C in 10% glycerol in small aliquots until used.

#### Chemical reconstitution of the Fe-S cluster on Cfd1 and Nbp35

The purified Nbp35 and Cfd1 proteins were dialyzed in 50 mM Tris-HCl, 150 mM NaCl, pH 8.0 to remove glycerol and rechecked their integrity and purity. Chemical reconstitution of Fe-S cluster on Nbp35 and Cfd1 was performed as described previously with some modifications [40–42]. Briefly, Nbp35 and

Cfd1 (100  $\mu$ M each protein) were reduced in reconstitution buffer (50 mM Tris-HCl, pH 8.0, 150 mM NaCl, 10 mM DTT) for 1 h at 25°C. Fresh anaerobic stocks solution of ferric ammonium citrate and Li<sub>2</sub>S were prepared in water containing 10 mM DTT before use and reconstitution of both proteins was started by the addition of 100  $\mu$ M ferric ammonium citrate and 100  $\mu$ M Li<sub>2</sub>S with stirring. To avoid precipitation, the reconstitution mixture was incubated with ferric ammonium citrate for 5 min before Li<sub>2</sub>S was added slowly drop wise to the reaction mixture followed by incubation of 2–3 hrs at 25°C. To remove non bound iron and sulphide, reconstituted proteins were desalted by PD-10 column equilibrated with reconstitution buffer containing 2 mM DTT. The assembly of Fe-S clusters into apo-proteins was monitored by UV-Vis spectroscopy (U3900, Hitachi, Japan).

#### Iron estimation

The iron content of Nbp35 and Cfd1 proteins were determined by the *O*-phenanthroline method as described previously [24,47]. Briefly, the Nbp35 and Cfd1 samples (80–100  $\mu$ l) were acidified by the addition of 3–5  $\mu$ l of concentrated HCl and then diluted with distilled water up to 0.2 ml. The mixtures were heated to 80°C for 10 mins and cooled down to room temperature. The reaction mixture was diluted with 0.6 ml of water, and 40  $\mu$ l of 10% hydroxylamine hydrochloride, 0.2 ml of 0.1% *O*-phenanthroline

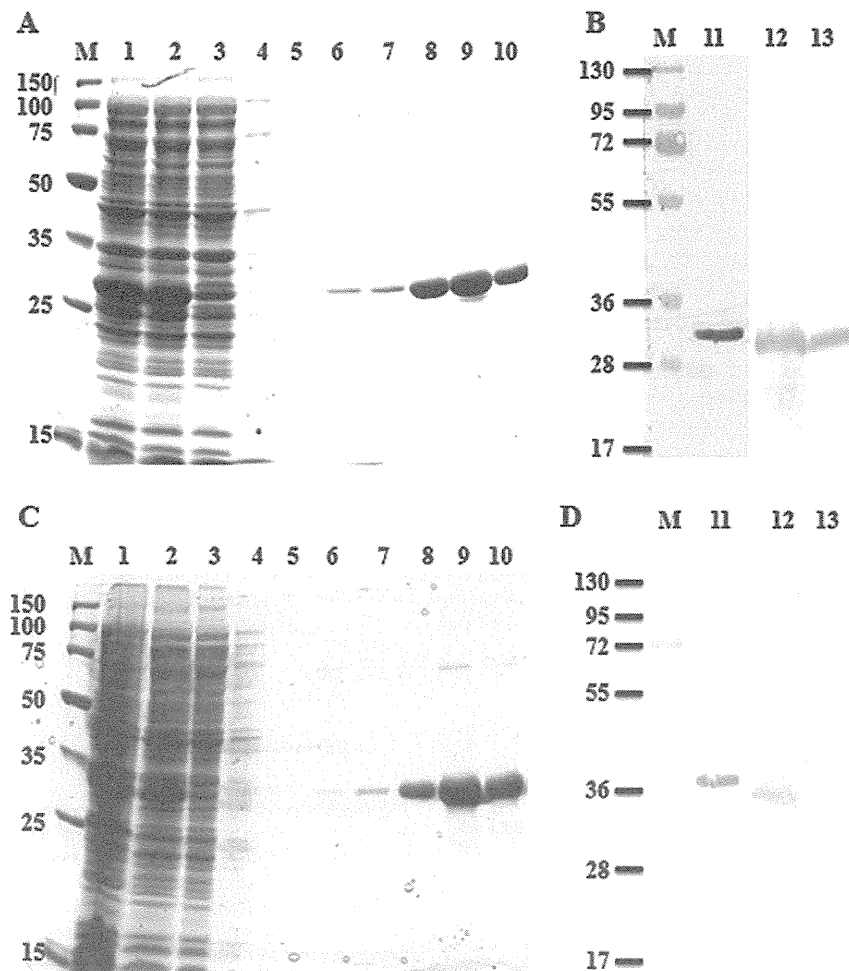


**Figure 6. Purification of recombinant Cfd1 and Nbp35 protein.** The recombinant Cfd1 protein was purified through Ni<sup>2+</sup>-NTA column. A) Lane M-marker, lane 1-total lysate, lane 2- supernatant, lane 3-flow through, lane 4-5-, 6-, & 7- wash (10, 20, 35, & 50 mM imidazole), lane 8- eluate (100 mM imidazole), lane 9- eluate (200 mM imidazole), lane 10- eluate (300 mM imidazole). B) Immunoblot was probed with anti-Cfd1 antibody. Lane M- represents molecular weight proteins marker, lane 11- purified rCfd1 protein was probed with anti-His monoclonal antibodies, lane 12- total *E. histolytica* cell lysate, and lane 13- supernatant of *E. histolytica* lysate C) Similarly, the recombinant Nbp35 protein was purified through Ni<sup>2+</sup>-NTA column Lane M-marker, lane 1- total lysate, lane 2- supernatant, lane 3- flow through, lane 4-5-, 6-, & 7- wash (10, 20, 35, & 50 mM imidazole), lane 8- eluate (100 mM imidazole) lane 9- (200 mM imidazole), lane 10- eluate (300 mM imidazole). D) Immunoblot was probed with anti-Nbp35 antibody. Lane M represents -molecular weight proteins marker, lane 11- purified rNbp35 protein was probed with anti-His monoclonal antibodies, lane 12- total *E. histolytica* cell lysate, and lane 13- supernatant of *E. histolytica* lysate. doi:10.1371/journal.pone.0108971.g006

were added. Finally, reaction mixtures were incubated at room temperature for 30 mins, and absorbance was measured at 512 nm.

#### Sulfide estimation

Sulfide content of purified rNbp35 and rCfd1 proteins was determined by measuring the absorbance of a blue colour complex treated with N,N-dimethyl-p-phenylenediamine dihydrochloride (DPD) as described previously [33]. Protein samples (50 µg) were diluted up to 775 µl with water and mixed with 50 µl of 6% NaOH. The DPD reagent (0.1%) dissolved in 5 N HCl (125 µl) and 30 mM FeCl<sub>3</sub> (50 µl) solutions were added to the reaction mixture and incubated for 30 min at 30°C. Finally, reaction mixture was vortexed, centrifuged for 5 mins at 13000 rpm to remove precipitate, and absorbance of supernatant was measured at 670 nm by UV-Vis spectroscopy (U3900, Hitachi, Japan). Na<sub>2</sub>S (0–100 µM) was used as standard.

#### Production of *E. histolytica* Nbp35 & Cfd1 antibodies and immunoblot analysis

Polyclonal antisera against recombinant *E. histolytica* Nbp35 or Cfd1 was raised in adult rabbit by three repeated subcutaneous injection. Pre-immune sera was collected before immunization and first dose of 300 µg Nbp35 or Cfd1 proteins emulsified in complete Freund's adjuvant was injected 8–10 places subcutaneously; followed by three booster doses of 250 µg of proteins emulsified in Freund's incomplete adjuvant. Anti-Nbp35 & Cfd1 titres were checked by ELISA after three weeks of final immunization. Finally, serum was collected from rabbits and stored at –30°C in small aliquots. Working antibodies were stored at 4°C. Prior animal ethical committee approval was taken and recommendations were strictly followed.

Cell lysate of *E. histolytica* (~1×10<sup>7</sup> cells/ml) was prepared using lysis buffer (100 mM Tris-HCl, pH 8.0, 300 mM NaCl, 1.0 mM EDTA, 1.0 mM DTT, 10% glycerol) as described

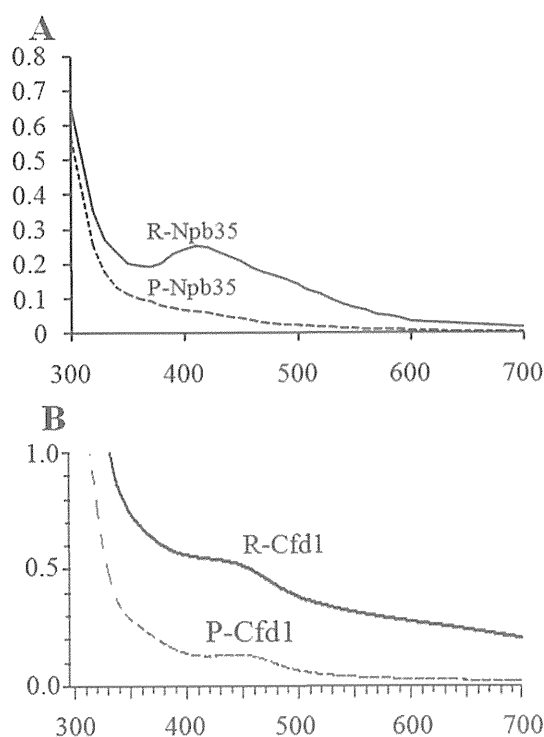


**Figure 7. UV-Visible spectra of purified and reconstituted rNbp35 and rCfd1 proteins.** A) As purified rNbp35 and rNbp35 after chemical reconstitution was scanned in the UV-Vis range to detect Fe-S cluster. Solid and dashed lines represent reconstituted Nbp35 and purified Nbp35, respectively. B) UV-visible spectra of purified rCfd1 and reconstituted rCfd1 protein in which, solid and dashed lines represent reconstituted rCfd1 and purified rCfd1, respectively.  
doi:10.1371/journal.pone.0108971.g007

previously [24]. The protein fractions were resolved by 10% SDS-PAGE and electro-blotted on to nitrocellulose membrane. The membrane was probed with polyclonal anti-Nbp35 or Cfd1 sera (1:2000) raised in rabbit as mentioned above. ALP-conjugated goat anti-rabbit IgG (1:2000) was used as secondary antibody and blot developed with BCIP/NBT (Santa Cruz), as per manufacturer's instructions [48].

#### Homology modelling and Structure Validation

Prediction of an interacting complex was proceeded with homology modelling, since the crystal structures for Nbp35 and Cfd1 are not available. Full length amino acid sequences of both the proteins were retrieved from Universal Protein Resource Database (<http://www.uniprot.org/>). The low percentage of sequence identity in the homologues PDB structures may not fetch robust models for protein structure. Thus, we have relied upon Zhang's I-TASSER server (<http://www.zhanglab.ccmb.med.umich.edu/I-TASSER/>), which gives the best protein models at the Critical Assessment of Structure Prediction (CASP 7 and CASP 8), a community-wide, worldwide experiment designed to obtain an objective assessment of the state-of-the-art in structure prediction [49]. Five models of Nbp35 and Cfd1 were computationally generated using the I-TASSER algorithm. The models were selected with lowest DOPE Score and verified using the Profile 3D profile analysis method [50]. The stereo-chemical properties of both the models were investigated with Ramachandran plot using PROCHECK [51]. The quality of final model was checked using Verify-3D program [52]. In addition to this, stereo

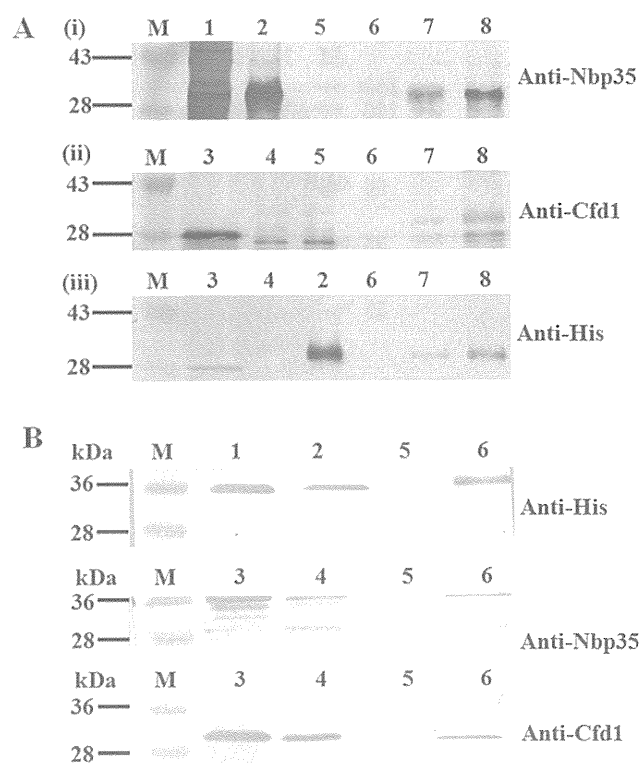


**Figure 8. Interaction study between Cfd1 and Nbp35 proteins.** (A) Co-purification using recombinant Nbp35 and thrombin digested Cfd1; Immunoblots of fractions obtained from co-purification experiment as described in material and methods probed with different antibodies (i) Anti-Nbp35 (ii) Anti-Cfd1 (iii) Anti-His antibodies for interaction between recombinant Nbp35 and thrombin digested Cfd1 proteins. Lane M- represents molecular weight proteins marker, lane 1- *E. coli* lysate overexpressing rNbp35, lane 2- purified rNbp35, lane 3- undigested rCfd1, lane 4- digested rCfd1, lane 5- wash (60 mM imidazole), lane 6 final wash did not show any proteins in all blots, lane 7- eluate (200 mM imidazole), lane 8- eluate (500 mM imidazole). (B) Pull down assay using rNbp35 and *E. histolytica* lysate: Ni<sup>2+</sup>-NTA bound rNbp35 was incubated with *E. histolytica* lysate as described in material and methods for pull down assay and eluate (500 mM imidazole) fraction was subjected to immunoblot analysis probed different antibodies (upper panel) Anti-His (middle panel) Anti-Nbp35 (lower panel) Anti-Cfd1 antibodies for rNbp35 and endogenous amoebic Cfd1 interaction. Lane M- represents molecular weight proteins marker, lane 1- total *E. coli* lysate expressed rNbp35, lane 2- supernatant rNbp35, lane 3- total amoebic lysate, lane 4- amoebic lysate flow through, lane 5 final wash did not show any proteins in all blots, lane 6- eluate (500 mM imidazole).  
doi:10.1371/journal.pone.0108971.g008

chemical qualities of 3D model were analyzed using WHATIF and ProSA web server. Molecular dynamics (MD) simulations were conducted for the Nbp35 and Cfd1 models in explicit solvent using the GROMACS 4.0.3 (The Groningen Machine for Chemical Simulations) package. The model was solvated by water molecules in an octahedron box having edges at a distance of 0.9 nm from the molecule's periphery. The solvated system was subjected to further energy minimization to remove the steric conflicts between the atoms of protein and water molecules having a maximum step of 2000 with steepest descent integrator that converge the energy minimization when the maximum force is smaller than 1000 kJ.mol<sup>-1</sup>.nm<sup>-1</sup>. The energy minimized model was subjected to position-restrained MD with NPT ensemble keeping number of particles (N), system pressure (P) and temperature (T) as constant parameters. This was carried out for 50,000 steps for a total of

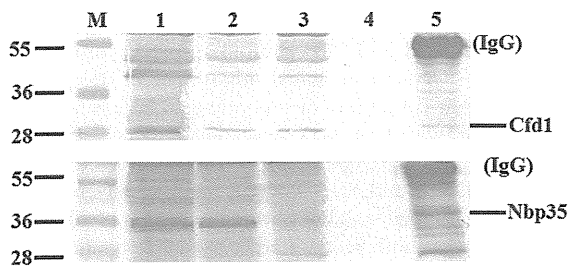


**Figure 9. In-vivo interaction study Nbp35 and Cfd1 by immunoprecipitation.** The anti-Nbp35 antibody bound with protein-A sepharose was incubated with amoebic lysate and immunoprecipitate was analysed by immunoblots were developed separately with anti-Cfd1 (upper panel) and anti-Nbp35 (lower panel) antibodies. IgG heavy chain (55 kda) and Cfd1 (29 Kda) were found in I.P. complex fraction and IgG heavy chain (55 kda) and Nbp35 (35 kda) bands found when probed with anti-Nbp35 antibody. Lane M- represents molecular weight proteins marker, lane 1- total amoebic lysate, lane 2- supernatant of amoebic lysate, lane 3- amoebic lysate flow through, lane 4- final wash did not show any proteins, lane 5- I.P. complex. doi:10.1371/journal.pone.0108971.g009

100 ps time period. Final MD was carried out for 3000 ps (3 ns) under Particle Mesh Ewald (PME), electrostatics in NPT condition [53].

#### Protein Protein Docking and complex simulation

It would be interesting to investigate whether Nbp35 and Cfd1 interact to each other and form complex in *E. histolytica*. Protein docking between Nbp35 and Cfd1 was done using PatchDock server (<http://bioinfo3d.cs.tau.ac.il/PatchDock/>) [54] with default settings. This server is widely used for the protein-protein docking studies [54–56] and its algorithm based on rigid docking with surface flexibility addressed by intermolecular penetration. PatchDock calculation resulted in three-dimensional transformations of the protein's Cartesian coordinate, which were further refined and scored based on protein-protein interaction energy using Fire Dock algorithm. Complex structure with the lowest interaction energy was taken as the final model for further analysis. Molecular dynamics simulations of Nbp35-Cfd1 complex was performed using the GROMACS 4.0.3 under gromos43a1 force field. The whole simulation experiment was done for 10 ns with 36527 water molecules and 1 Na<sup>+</sup> ion. The same methodology was adopted for simulation of this complex as done in the MD of individual proteins Nbp35 and Cfd1.

#### Co-purification by affinity chromatography

*In vitro* interaction between recombinant Nbp35 and Cfd1 proteins was investigated by co-elution from an affinity column [57]. The bacterial cell pellet overexpressing recombinant Nbp35 protein was dissolved in 10 ml lysis buffer (50 mM Tris-HCl, pH 8.0, 300 mM NaCl, 0.1% triton X-100) supplemented with 1.0 mM PMSF, 1 X protease inhibitor cocktail (100 µl) and 100 µg/ml lysozyme, and incubated at 30°C for 45 mins. The cell suspension was sonicated on ice and lysate centrifuged at 13000 rpm for 20 min at 4°C. The supernatant containing Nbp35 with N-terminal His-tag was loaded onto a Ni<sup>2+</sup>-NTA column and washed with buffer A (50 mM Tris-HCl, pH 8.0, 300 mM NaCl, 0.1% Triton X 100) containing 10–50 mM imidazole to remove unbound proteins. Purified recombinant Cfd1 protein was digested with thrombin to remove N-terminal-His-tag and eluted from column followed by desalting as described earlier [24]. The digested Cfd1 protein was loaded on the Nbp35

bound Ni<sup>2+</sup>-NTA column and incubated for 1.0 hr at RT followed by washing with 15 ml each of buffer A containing 10–60 mM imidazole. Finally, column-bound proteins complex was eluted with buffer A containing 200 and 500 mM of imidazole. Eluate proteins complex was analyzed by 10% SDS-PAGE and western blotting [48] with anti-His (1:2000 Santa cruz), anti-Nbp35 (1:2000), and anti-Cfd1 (1:2000) antibodies raised in rabbit as described previously.

#### Interaction between recombinant protein and amoebic cell lysate

The bacterial cell pellet over-expressing recombinant Nbp35 protein was processed to obtain Nbp35 bound to Ni<sup>2+</sup>-NTA column as described in the above section. Amoebic cell lysate (~5 × 10<sup>7</sup> cells) was mixed with Ni<sup>2+</sup>-NTA matrix bound Nbp35 in column and incubated for 1 hr at 25°C for complex formation. The column was washed rigorously with buffer A containing 10–50 mM imidazole to remove the unbound amoebic proteins and bound proteins complex was eluted with buffer A containing 200 & 500 mM imidazole. All the fractions were electrophoresed in 12% SDS-PAGE and transferred to nitrocellulose membrane. The blots were probed with different antibodies; Anti-His (Santa cruz) mouse monoclonal antibody, anti-Nbp35 & anti-Cfd1 antibodies raised in rabbit at 1:2000 dilution. The alkaline phosphatase conjugated anti-rabbit secondary antibody or anti mouse were also used at 1:2000 dilution and finally blots were developed by adding BCIP/NBT solution as per manufacturer's instruction.

#### Interaction study by immunoprecipitation

The immunoprecipitation experiments were performed using standard protocol [48] with minor modifications. The anti-Cfd1 or anti-Nbp35 antibody (10 µl) was incubated with protein A sepharose beads (100 µl) overnight at 4°C. The beads suspension was centrifuged at 500 × g for 2 mins at 4°C, supernatant discarded and pellet fraction washed twice with 1.0 ml PBS. Amoebic cell lysate (~5 × 10<sup>7</sup> cells) was then mixed with antibody bound protein A sepharose matrix in a 1.5 ml tube with gentle mixing of the sample on a suitable shaker and incubated for 90 mins at RT or overnight at 4°C. The mixture was centrifuged at 500 × g for 2 mins at 4°C, supernatant discarded and matrix washed twice with 1 ml PBS to remove loosely bound proteins. The bound complex was eluted from beads by boiling in 100 µl of 1 × SDS-loading dye for 10 mins at 95°C. Finally, immunoprecipitated complex (I.P.) was collected by centrifugation at 13000 rpm for 30 sec at RT and supernatant applied on 12% SDS-PAGE and transferred to nitrocellulose membrane. The blots were probed with different antibodies as described above & developed by BCIP/NBT solution [48].

## Results and Discussion

#### Modelling of Nbp35 protein

BLASTP search against Protein Data Bank (PDB) using Nbp35 as query sequence did not give any suitable template. The crystal structure of nucleotide-binding protein from *Archaeoglobus fulgidus* (PDB ID: 2PH1\_A) shared only 36% sequence identity and 70% query coverage. Large portion of the target sequence remained unaligned which suggested that not so many nucleotide-binding protein structures have been experimentally resolved to date. Five model of Nbp35 were generated using the I-TASSER algorithm which directly modelled the aligned regions from the template structures (2ph1\_A & 3vx3\_A) and the unaligned regions modelled with ab-initio simulations. These models of Nbp35 were generated with C-scores ranging from -1.99 to -3.04. The C-



score is a confidence score and ranges from  $-5$  to  $2$ , with higher scores representing higher confidence in the model [49]. Best three models were selected (M1, M2 and M3) based on their C-scores ( $-1.99$ ,  $-2.65$  and  $-2.84$ , respectively). Discrete optimized protein energy (DOPE) suggested that the second model (M2) revealed the lowest energy ( $-33600.3349$ ) whereas the other two models DOPE score, i.e., M1 and M3 revealed  $-33217.539063$  and  $-32761.363281$ , respectively. The  $\Phi/\Psi$  distribution of the backbone conformational angle for each residue of the selected structures was calculated. The M1 model revealed the highest 96.7% residues in the most favoured region and additional allowed region. 2.2% residues were found in generously allowed region whereas only 1.1% residues (Leu232, Thr274 and His275) fell in disallowed region. Based on the DOPE score and the Ramachandran plot, the M2 model was considered to be a reliable model used for rest of the study. After loop refinement, final structure with the lowest energy was checked by Profile-3D (DS 2.5). The self-compatibility score for this protein is 133.09 which is much higher than the Verify expected lowest score (68.24) and very close to the Verify expected high score (151.65). Validation of the modelled protein with ProSA-web revealed that the Z score ( $-6.74$ ) is within the range of native conformations of the crystal structures. The plot showed the energy remains negative for almost all amino acid residues indicating the acceptability of the predicted model. The Verify-3D result of the model showed that 98.80% amino acids had an average 3D-1D score, and thus indicated the reliability of the proposed model. The monomeric Nbp35 is an  $\alpha/\beta$  type protein containing P-loop nucleoside triphosphate hydrolase type domain (70–314). The modelled structure composed of 12  $\alpha$ -helices ( $\alpha_1$ – $\alpha_{12}$ ) and four-stranded parallel  $\beta$ -sheets ( $\beta_1$ ,  $\beta_2$ ,  $\beta_4$ ,  $\beta_5$ ) with one anti-parallel  $\beta$ -sheet ( $\beta_3$ ). One  $\beta/\alpha/\beta$  motif ( $\beta_1/\alpha_4/\beta_2$ ) is present in between two  $\alpha$ -helices ( $\alpha_2$  and  $\alpha_5$ ). ATPase-like, ParA/MinD signature motif (191–272) is formed by a central  $\alpha$ -helix ( $\alpha_8$ ) joined with a  $\beta$ -sheet ( $\beta_5$ ) and  $\alpha$ -helix ( $\alpha_9$ ) on either side.

### Modelling of Cfd1 protein

In order to proceed for an accurate search of interacting residues of Cfd1, it is indeed necessary to have a robust 3D model of the protein structure. BLASTp search against PDB database did not return any suitable template. Five model were generated (2ph1\_A & 3vx3\_A as template) using I-TASSER web server with C-score ranging from  $-1.61$  to  $-3.52$ . The fourth loop refined model (C-score =  $-3.26$ ) revealed the lowest DOPE score ( $-23306.49$ ) and only three residues; Lys20, Val153 and Asn91 fell in disallowed region. The Ramachandran map of the model revealed 95.2% residues in the most favoured region and additional allowed region. The self-compatibility score for this protein is 87.68, which is much higher than the Verify expected lowest score (55.85). The further precision of the model was checked using the ProSA server, where the Z-score ( $-6.46$ ) depicts the model to be within the domicile of reported X-ray crystal structures till date. Moreover, the Verify-3D results illustrated the compatibility score of  $\sim 84\%$  of amino acid residues which assesses the favourability of residue environments within the folded structure. All these validations suggested the robustness and reliability of the proposed model. The modelled Cfd1 is an  $\alpha$ -helices dominated protein (8  $\alpha$ -helices and 2  $\beta$ -sheets) containing P-loop nucleoside triphosphate hydrolase type domain (21–211). A central  $\alpha$ -helix is present in CobQ/CobB/MinD/ParA nucleotide binding domain, joined by one  $\alpha$ -helix ( $\alpha_4$ ) and one  $3_{10}$  helix on either side.

### Molecular dynamics simulation of Nbp35 & Cfd1 proteins

The simulated Nbp35 and Cfd1 showed an initial jump in the rmsd at 0 ps time, depicts the initial adjustment of the protein model in the solvent condition corresponding to energy minimization and equilibration steps. MD simulations analysis of Nbp35 showed the root mean squared deviation (RMSD) trajectory rose from 0.0 ps to 2000 ps and then attained final stability, whereas Cfd1 model attained final stability after 2400 ps (Fig. 1). Further analysis suggested that both proteins achieved stable confirmation after simulations. After a precise validation protocol for the projected all-atomic simulated 3D model, the protein complex was processed for MD simulations in the explicit solvent condition. All atoms (RMSD) of the modeled system was checked against the time scale as shown in Fig. 2a, regarding its stability which showed the system attained final stability within average fluctuation of 0.4 nm. We have further analyzed complex stability of Nbp35-Cfd1 in the presence of hydrogen bonds and found very small fluctuation within the complex as compared to complex with water. The root mean square fluctuations (RMSF) plot for the model system depicts the same stability feature (Fig. 2b) and is well correlated with the RMSD plot. Interestingly, Cfd1 showed more flexibility for residues in the range of 35–55 and 150–250 residue numbers, whereas Nbp35 showed flexibility for residues in the range of 1–60, 130–155, 260–270, and 310–315 residue numbers. All these flexibility of residues were expected to be engaged in protein-protein interaction (Fig. 2b).

### *In-silico* protein-protein Interaction study

Protein-protein complex model of Nbp35-Cfd1 as obtained from Patchdock was processed for MD simulations with Newton's laws of motion in explicit solvent conditions. Ever since the algorithm so far developed for an accurate prediction of large biomolecular complex using docking methods is limited to steric and electrostatic compatibility between docking partners. The approach which has been adopted in the present study indicates an apparent prediction of interaction between these proteins. The protein complex shows few structural regions that are responsible for making protein-protein complex formation, possible by virtue of Van der Waals interactions. Further analysis showed the amino acids involved in contacts, viz. Phe33-Lys35, Gly131-Val135 and Ile147-Glu151 of Nbp35; Gly5-Val6, Met34-Asp39 and Gly46-Ala52 of Cfd1 (Fig. 3a). The complex simulation seems to have a converged trajectory, which has been plotted for protein amino-acids, backbone atoms and side chain atoms as a function of time (Fig. 2a). The prime objective of adopting molecular modeling is not to access the exact behavior of proteins in complex state over time period but to tract the stochastic motional behavior of both proteins in complex state. The loops involved in making the proteins complex are found to be in contact throughout the simulation. The main driving force, as found in this study, is Van der Waals interactions that are responsible for association of both proteins for execution of corresponding biological functions. On the other hand, the polar interactions are not found to be important for this protein complex. This had been assessed by taking into account of the hydrogen bonds which were formed between the protein atoms in the complex state and remains constant throughout the simulations. Similar results were also found while accessing the number of hydrogen bonds formed by protein atoms (in complex state) with the water molecules, which are also constant throughout the simulations. Thus, these findings strengthen our observations that hydrophobic forces surpass over hydrophilic forces between Nbp35 and Cfd1 proteins (Fig. 4a). Interestingly, when solvent accessible surface areas (SASA) calculated over the recorded trajectory frames from MD

simulations as a function of time, showed a decrease of almost 15–20 nm.S<sup>2</sup>.N<sup>-1</sup> as shown in (Fig. 4b). This observation demonstrates that the globular folding of proteins get more compact, thereby preserving the hydrophobic residues from getting exposed to the solvent in complex state.

The conformational changes of protein complex were also analyzed by MD simulations in terms of Principal components analysis (PCA), where we have taken into consideration of the first eigenvectors, to trace down the movement of macromolecule. Pcmdump was used to prepare the average coordinates from simulation and was used to show the projections of eigenvectors. The approach helps us in correlating the related fluctuations of protein atoms with that of the total fluctuation in the course of simulation. Fig. 3b represents a porcupine plot for backbone atoms (represented in green color) and the red spikes represent the directionality regarding the motional behavior. The structural regions those are in contacts at the interface both of the proteins are shown an enclosed box in Fig. 3b. We also analyzed the polar contacts formed between these two proteins, by analyzing the coordinate files at regular interval from MD trajectory, though the numbers of hydrogen bond remains same but the residues participating varies. An overview of the residue pairs that are in contact, had been generated based upon the average structure and is represented by Contact-map in Fig. 5. Thus, the fundamental observation as found from the simulation study, being the hydrophobic forces, i.e. the Van der Waals interaction plays crucial role in making the protein complex stable, even in the explicit solvent conditions.

#### Expression and purification of recombinant Cfd1 and Nbp35

The *Nbp35* ORF of 1002 nucleotides encodes a 333 amino acids protein with predicted molecular weight ~36 kDa and an iso-electric point (pI) value 6.05. The Nbp35 protein, related to Cfd1 show 49% amino acid identity with yeast Nbp35 protein [30]. Similarly, the *Cfd1* ORF of 822 nucleotides encodes a 273 amino acids protein with predicted molecular weight ~29 kDa and an iso-electric point (pI) value 4.98. Neither the MITO-PROT II program nor Signal IP 4.1 Server, which predicts protein localization in cells, and a Kyte-Doolittle hydrophathy plot, suggested any possible cellular localization other than cytosolic distribution for Nbp35 and Cfd1 proteins. The recombinant (rNbp35 and rCfd1) proteins were expressed in *E. coli* BL21 (DE3) and purified to homogeneity using Ni<sup>2+</sup>-NTA affinity chromatography as shown in Fig. 6. It was observed that rCfd1 expression was higher in soluble form and eluted between 100–400 mM imidazole with high protein yield of ~5 mg/ml. The purified rCfd1 protein gave a single band of ~29 kDa when examined on SDS-PAGE and immunoblot using anti-Cfd1 antibody in parasite lysates (Fig. 6a). Similarly, Nbp35 was also expressed and purified to homogeneity using Ni<sup>2+</sup>-NTA affinity chromatography (Fig. 6b). It revealed an apparently homogeneous band of 38 kDa on 12% SDS-PAGE that correlates well with predicted molecular mass 36 kDa. The purified rNbp35 and rCfd1 proteins concentration determined by Bradford's method was found to be 0.212 mg/ml (rCfd1), 0.187 mg/ml (rNbp35) and were stable at -80°C for more than six months in the presence of 10% glycerol.

Polyclonal antisera against purified rNbp35 & rCfd1 proteins were raised in adult rabbit showed high titre at final bleed (1:16000 dilution). Antibody against either rNbp35 or rCfd1 recognised a specific and single band both in *E. histolytica* lysate proteins and purified recombinant protein suggesting that a single homologue is present in the parasite (Fig. 6a & 6b). By immunoblot analysis of a series of diluted recombinant proteins

(data not shown), we roughly estimated that the *E. histolytica* contains a significant amount of Nbp35 & Cfd1, which consists of approximately 0.01–0.02% of the total proteins.

#### Biochemical properties of Nbp35 and Cfd1 proteins

The ability to coordinate Fe-S cluster and donate cluster to apo target proteins is a conserved feature of members of the ApbC/Nbp35 family. Cfd1 (present in yeast and *E. histolytica*) shares similarities with, and falls into, the subfamily of P-loop ATPases [58,59]. The purified Nbp35 and Cfd1 proteins were colourless which indicates loss of cluster during purification. The UV-visible spectrum of purified Nbp35 did not show pronounced absorbance at ~400 nm as compared to purified Cfd1 which suggests that Nbp35 clusters are more labile in the presence of oxygen. We therefore, reconstituted Fe-S clusters of Nbp35 and Cfd1 proteins under reduced conditions as described in the material and methods. The reconstituted spectra of Nbp35 (Fig. 7a) and Cfd1 (Fig. 7b) showed a peak around 410 nm which is characteristic of [4Fe-4S] cluster. We also estimated iron and sulphide content of both purified proteins just after purification and found that rNbp35 and rCfd1 holds 200–253 μM & 56–87 μM of iron and 209±06 μM & 78±12 μM sulfide, respectively. Thus, the results suggest that rNbp35 & rCfd1 hold two [4Fe-4S] & one [4Fe-4S] cluster, respectively.

Interestingly, *in vitro* assembly and transfer of Fe-S clusters on these P-loop NTPases did not required nucleotide binding or hydrolysis. However, in yeast, nucleotide binding and hydrolysis are required for Fe binding to Cfd1 and Nbp35 *in vivo* [41]. In yeast (*S. cerevisiae*), the C-terminal domains of scNbp35 and scCfd1 proteins are similar. The C-terminal domain of scNbp35 holds a 4Fe-4S cluster. The mutational study on scCfd1 and scNbp35 proteins has shown that two central cysteine residues (CPXC) of the C-terminal motif are crucial for the co-ordination of the labile [4Fe-4S] clusters and the formation of the Cfd1-Nbp35 hetero-tetramer complex formation, and the viability of the yeast cells [40]. Nbp35 has the capacity to bind a ferredoxin-like [4Fe-4S] cluster at the N-terminus of each monomer and a single [4Fe-4S] cluster bridging a Nbp35 dimer through the conserved CX2C motif near the C-terminus of each monomer [40]. It has been suggested that the N-terminal ferredoxin-like cluster on Nbp35 is structural and not subject to transfer to downstream targets, while the C-terminal bridged clusters are transferred to target proteins [40]. In addition, previous work had also shown that when co-expressed in *E. coli*, Cfd1 and Nbp35 form a heterotetrameric complex that bound four [4Fe-4S] clusters upon reconstitution *in vitro* [41]. Above all, the functional relevance of the Cfd1 and Nbp35 lies in the ability to assemble and deliver Fe-S clusters in the cytosol [34,41].

#### *In-vitro* and *in-vivo* protein-protein interaction study

To prove *in-silico* interaction, we performed co-purification and immunoprecipitation experiments. Co-purification using *E. coli* rNbp35 lysate and thrombin digested rCfd1 was performed as described in materials and methods and immunoblot analysis of different fractions with anti-Nbp35 and anti-Cfd1 antibodies confirmed the presence of the Nbp35-Cfd1 protein complex in the eluate fractions. Anti-Cfd1 probed blot (Fig. 8a, ii) showed a relatively faint band of digested rCfd1 protein in the eluate fractions (lane 7 & 8) which corresponded to thrombin digested rCfd1 in the input and flow through fractions (lane 4 & 5). Notably, no Cfd1 was detected in the final wash fraction (lane 6) indicating complete removal of any unbound/loosely bound Cfd1 protein. The undigested rCfd1 (lane 3) was observed to be slightly higher than digested rCfd1 in other fractions due to thrombin

mediated cleavage of His tag. Similarly, anti-Nbp35 probed blot (Fig. 8a, i) recognised rNbp35 in the eluate fractions (lane 7 & 8) which corresponded to rNbp35 in *E. coli* lysate overexpressing fraction (lane 1) and purified rNbp35 fraction (lane 2). Again, rNbp35 was not detected in either the digested Cfd1 flow through fraction (lane 5) or final wash fraction (lane 6) indicating complete removal of any unbound/loosely bound rNbp35 protein before elution. To further confirm our results, we probed the same fractions with anti-His antibody (Fig. 8a, iii) which recognised undigested rCfd1 (lane 3), purified rNbp35 (lane 2) as well as rNbp35 in the eluate fractions (lanes 7, 8) whereas digested Cfd1 was not detected in the eluate fractions (lane 7, 8). This shows that Cfd1 co-eluted with rNbp35 in the eluate fraction lacked a his-tag and therefore co-elution is solely due to complex formation with rNbp35 (Fig. 8a, ii). Thus, these results indicate that Nbp35 and Cfd1 interact with each other and form a stable complex supporting our *in-silico* analysis.

The *in-vitro* result was further verified under *in-vivo* conditions by pull down assay using purified rNbp35 protein and *E. histolytica* total lysate, as described in materials and methods section. All the fractions were run on 12% SDS-PAGE and immunoblot probed with anti-His, anti-Nbp35 or anti-Cfd1 antibodies. As shown in Fig. 8b, both anti-His (Fig. 8b, upper panel) and anti-Nbp35 antibody (Fig. 8b, middle panel) detected Nbp35 in the pull down eluate fraction as well as the input (lane 1 & 3) and flow through fraction (lane 2 & 4) which shows that rNbp35 overexpressed in *E. coli* binds with Ni<sup>+2</sup>-NTA agarose and gets eluted in eluate fraction similar to any other conventional his tagged fusion protein. *E. histolytica* cell lysate possesses endogenous Nbp35 and Cfd1 proteins without His-tag. Immunoblot probed with anti-Cfd1 antibody (lower panel) detected a band for co-eluted Cfd1 in the pull down eluate fraction (lane 6) which corresponded to endogenous Cfd1 in the amoebic lysate (lane 3) and amoebic lysate flow through fraction (lane 4). This shows that endogenous Cfd1 in the lysate was retained by Ni<sup>+2</sup>-NTA bound rNbp35 even after extensive washing and co-eluted with rNbp35. No band was observed in final wash fraction (Fig. 8b, lane 5) which indicates that all unbound/loosely bound proteins were completely washed away. Thus, pull down assay using *E. histolytica* lysate and rNbp35 proteins shows that Cfd1 protein present in *E. histolytica* cell lysate forms a complex with recombinant Nbp35 by physical interaction between these two proteins and hence pulled down.

Finally, immunoprecipitation with either anti-Nbp35 or anti-Cfd1 antibodies was performed to confirm *in-vivo* interaction between these two proteins. Initially, anti-Nbp35 antibody was used to pull down its partner protein from *E. histolytica* lysate and blot probed with anti-Cfd1 antibody. As shown in Fig. 9 (upper panel), Cfd1 protein was detected in the eluate fraction (lane 5). Similarly, Nbp35 protein was detected in the eluate fraction

(Fig. 9, lower panel, lane 5) when anti-Cfd1 antibody was used for pull down. The intense band of 55 kDa corresponds to IgG heavy chain of antibody. We have also detected 2 faint bands, one above Nbp35 and one below Cfd1 with anti-Nbp35 antibody but not with anti-Cfd1 antibody which is probably due to cross reactivity of anti-Nbp35 antibody with other proteins. Although at present, we could not rule out the possibility of other interacting proteins. Thus, our results clearly demonstrate that these two *E. histolytica* proteins, Nbp35 and Cfd1, physically interact with each other to form a stable complex *in vivo*. A similar interaction between these two proteins has been previously reported in yeast [40,41] where they work together to transfer preassembled Fe-S clusters on cytosolic apo-Fe-S proteins. Our reconstitution as well as interaction results favours a similar role for Nbp35 and Cfd1 in *E. histolytica* but the presence of NIF system in place of ISC system for Fe-S cluster assembly in this parasite demands further study on this unique model organism as far as Fe-S cluster assembly mechanism is concerned.

## Conclusion

In the present study the two proteins Nbp35 and Cfd1 were cloned, expressed and recombinant fusion proteins purified by affinity column chromatography. Our *in-silico* molecular dynamics simulation studies, *in vitro* pull down assay as well as *in vivo* immunoprecipitation results clearly indicate an interaction between Nbp35 and Cfd1 proteins of CIA machinery to form a stable complex. This interaction may be essential initial step for transfer of preassembled Fe-S clusters on Nbp35-Cfd1 complex through Nar1-Cial proteins to target apo-proteins in the non-mitochondrial compartment of *E. histolytica*. However, CIA and NIF machineries co-exist in the cytoplasm with completely different antecedents but how they crosstalk remains to be elucidated.

## Acknowledgments

We thank Dr. Sandipan Ganguly, Laboratory of Molecular Parasitology, NICED, Kolkata, India for providing *E. histolytica* culture. We also thank other Ph. D. students Asif Eqbal, Shshi, and Kuljeet for their support and discussion. Shadab (DBT-SRF), K. P. Singh (DST INSPIRE SRF-P), & Amir Zaidi (CSIR-SRF) acknowledge the financial assistance in the form of fellowship support from DBT, DST & CSIR, New Delhi, India.

RMRIMS communication No. RMRI/016/Pub/Dated 07/03/2014  
Ethics Statement: "N/A"

## Author Contributions

Conceived and designed the experiments: SA MRD VA. Performed the experiments: SA MRD RK AZ KPS. Analyzed the data: SA MRD KPS GCS VA. Contributed reagents/materials/analysis tools: AKR PD TN VA. Wrote the paper: SA MRD KPS VA.

## References

- Clark CG, Roger AJ (1995) Direct evidence for secondary loss of mitochondria in *Entamoeba histolytica*. *Proc-Natl-Acad-Sci-U-S-A* 92: 6518–6521.
- Tovar J, Fischer A, Clark CG (1999) The mitosome, a novel organelle related to mitochondria in the mitochondrial parasite *Entamoeba histolytica*. *Mol Microbiol* 32: 1013–1021.
- Susin SA, Lorenzo HK, Zamzami N, Marzo I, Snow BE, et al. (1999) Molecular characterization of mitochondrial apoptosis-inducing factor. *Nature* 397: 441–446.
- Lill R, Kispal G (2000) Maturation of cellular Fe-S proteins: an essential function of mitochondria. *Trends Biochem Sci* 25: 352–356.
- Beinert H, Holm RH, Munck E (1997) Iron-sulfur clusters: nature's modular, multipurpose structures. *Science* 277: 653–659.
- Lill R, Muhlenhoff U (2005) Iron-sulfur-protein biogenesis in eukaryotes. *Trends Biochem Sci* 30: 133–141.
- Lill R, Muhlenhoff U (2008) Maturation of iron-sulfur proteins in eukaryotes: mechanisms, connected processes, and diseases. *Annu Rev Biochem* 77: 669–700.
- Lill R, Hoffmann B, Molik S, Pierik AJ, Rietzschel N, et al. (2012) The role of mitochondria in cellular iron-sulfur protein biogenesis and iron metabolism. *Biochim Biophys Acta* 1823: 1491–1508.
- Kispal G, Csere P, Prohl C, Lill R (1999) The mitochondrial proteins Atm1p and Nfs1p are essential for biogenesis of cytosolic Fe/S proteins. *EMBO J* 18: 3981–3989.
- Muhlenhoff U, Balk J, Richhardt N, Kaiser JT, Sipos K, et al. (2004) Functional characterization of the eukaryotic cysteine desulfurase Nfs1p from *Saccharomyces cerevisiae*. *J Biol Chem* 279: 36906–36915.
- Nakai Y, Umeda N, Suzuki T, Nakai M, Hayashi H, et al. (2004) Yeast Nfs1p is involved in thio-modification of both mitochondrial and cytoplasmic tRNAs. *J Biol Chem* 279: 12363–12368.

12. Lill R (2009) Function and biogenesis of iron-sulphur proteins. *Nature* 460: 831–838.
13. Balk J, Pilon M (2010) Ancient and essential: the assembly of iron-sulfur clusters in plants. *Trends Plant Sci* 16: 218–226.
14. Rouault TA (2012) Biogenesis of iron-sulfur clusters in mammalian cells: new insights and relevance to human disease. *Dis Model Mech* 5: 155–164.
15. Craig EA, Voisine C, Schilke B (1999) Mitochondrial iron metabolism in the yeast *Saccharomyces cerevisiae*. *Biol Chem* 380: 1167–1173.
16. Muhlenhoff U, Lill R (2000) Biogenesis of iron-sulfur proteins in eukaryotes: a novel task of mitochondria that is inherited from bacteria. *Biochim Biophys Acta* 1459: 370–382.
17. Tovar J, Leon-Avila G, Sanchez LB, Sutak R, Tachezy J, et al. (2003) Mitochondrial remnant organelles of *Giardia* function in iron-sulfur protein maturation. *Nature* 426: 172–176.
18. Dolezal P, Smid O, Rada P, Zubacova Z, Bursac D, et al. (2005) *Giardia* mitochondria and trichomonad hydrogenosomes share a common mode of protein targeting. *Proc Natl Acad Sci U S A* 102: 10924–10929.
19. Tsaousis AD, Ollagnier de Choudens S, Gentekaki E, Long S, Gaston D, et al. (2012) Evolution of Fe/S cluster biogenesis in the anaerobic parasite *Blastocystis*. *Proc Natl Acad Sci U S A* 109: 10426–10431.
20. Changmai P, Horakova E, Long S, Cernotikova-Stribrna E, McDonald LM, et al. (2013) Both human ferredoxins equally efficiently rescue ferredoxin deficiency in *Trypanosoma brucei*. *Mol Microbiol* 89: 135–151.
21. Seeber F (2002) Biogenesis of iron-sulfur clusters in amitochondriate and apicomplexan protists. *Int J Parasitol* 32: 1207–1217.
22. Kumar B, Chaubey S, Shah P, Tanveer A, Charan M, et al. (2011) Interaction between sulphur mobilisation proteins SufB and SufC: evidence for an iron-sulphur cluster biogenesis pathway in the apicoplast of *Plasmodium falciparum*. *Int J Parasitol* 41: 991–999.
23. Ali V, Nozaki T (2013) Iron-sulfur clusters, their biosynthesis, and biological functions in protozoan parasites. *Adv Parasitol* 83: 1–92.
24. Ali V, Shigeta Y, Tokumoto U, Takahashi Y, Nozaki T (2004) An Intestinal Parasitic Protist, *Entamoeba histolytica*, Possesses a Non-redundant Nitrogen Fixation-like System for Iron-Sulfur Cluster Assembly under Anaerobic Conditions. *J Biol Chem* 279: 16863–16874.
25. Gill EE, Diaz-Trivino S, Barbera MJ, Silberman JD, Stechmann A, et al. (2007) Novel mitochondrion-related organelles in the anaerobic amoeba *Mastigamoeba balamuthi*. *Mol Microbiol* 66: 1306–1320.
26. Nyvtova E, Sutak R, Harant K, Sedimova M, Hrdy I, et al. (2013) NIF-type iron-sulfur cluster assembly system is duplicated and distributed in the mitochondria and cytosol of *Mastigamoeba balamuthi*. *Proc Natl Acad Sci U S A* 110: 7371–7376.
27. Müller M, Mentel M, van Hellemond JJ, Henze K, Woehle C, et al. (2012) Biochemistry and evolution of anaerobic energy metabolism in eukaryotes. *Microbiol Mol Biol Rev* 76: 444–495.
28. Sheftel A, Stehling O, Lill R (2010) Iron-sulfur proteins in health and disease. *Trends Endocrinol Metab* 21: 302–314.
29. Roy A, Solodovnikova N, Nicholson T, Antholine W, Walden WE (2003) A novel eukaryotic factor for cytosolic Fe-S cluster assembly. *EMBO J* 22: 4826–4835.
30. Hausmann A, Aguilar Netz DJ, Balk J, Pierik AJ, Muhlenhoff U, et al. (2005) The eukaryotic P loop NTPase Nbp35: an essential component of the cytosolic and nuclear iron-sulfur protein assembly machinery. *Proc Natl Acad Sci U S A* 102: 3266–3271.
31. Balk J, Pierik AJ, Netz DJ, Muhlenhoff U, Lill R (2004) The hydrogenase-like Nar1p is essential for maturation of cytosolic and nuclear iron-sulfur proteins. *EMBO J* 23: 2105–2115.
32. Balk J, Lobreaux S (2005) Biogenesis of iron-sulfur proteins in plants. *Trends Plant Sci* 10: 324–331.
33. Zhang Y, Lyver ER, Nakamaru-Ogiso E, Yoon H, Amutha B, et al. (2008) Dre2, a conserved eukaryotic Fe/S cluster protein, functions in cytosolic Fe/S protein biogenesis. *Mol Cell Biol* 28: 5569–5582.
34. Netz DJ, Stumpfig M, Dore C, Muhlenhoff U, Pierik AJ, et al. (2010) Tah18 transfers electrons to Dre2 in cytosolic iron-sulfur protein biogenesis. *Nat Chem Biol* 6: 758–765.
35. Van Wietmarschen N, Moradian A, Morin GB, Lansdorp PM, Uringa EJ (2012) The mammalian proteins MMS19, MIP18, and ANT2 are involved in cytoplasmic iron-sulfur cluster protein assembly. *J Biol Chem* 287: 43351–43358.
36. Stehling O, Vashisht AA, Mascarenhas J, Jonsson ZO, Sharma T, et al. (2012) MMS19 assembles iron-sulfur proteins required for DNA metabolism and genomic integrity. *Science* 337: 195–199.
37. Gari K, Leon Ortiz AM, Borel V, Flynn H, Skchel JM, et al. (2012) MMS19 links cytoplasmic iron-sulfur cluster assembly to DNA metabolism. *Science* 337: 243–245.
38. Stehling O, Mascarenhas J, Vashisht AA, Sheftel AD, Niggemeyer B, et al. (2013) Human CIA2A-FAM96A and CIA2B-FAM96B integrate iron homeostasis and maturation of different subsets of cytosolic-nuclear iron-sulfur proteins. *Cell Metab* 18: 187–198.
39. Broderick JB (2007) Assembling iron-sulfur clusters in the cytosol. *Nat Chem Biol* 3: 243–244.
40. Netz DJ, Pierik AJ, Stumpfig M, Muhlenhoff U, Lill R (2007) The Cfd1-Nbp35 complex acts as a scaffold for iron-sulfur protein assembly in the yeast cytosol. *Nat Chem Biol* 3: 278–286.
41. Netz DJ, Pierik AJ, Stumpfig M, Bill E, Sharma AK, et al. (2012) A bridging [4Fe-4S] cluster and nucleotide binding are essential for function of the Cfd1-Nbp35 complex as a scaffold in iron-sulfur protein maturation. *J Biol Chem* 287: 12365–12378.
42. Bych K, Netz DJ, Vigani G, Bill E, Lill R, et al. (2008) The essential cytosolic iron-sulfur protein Nbp35 acts without Cfd1 partner in the green lineage. *J Biol Chem* 283: 35797–35804.
43. Basu S, Leonard JC, Desai N, Mavridou DA, Tang KH, et al. (2013) Divergence of Erv1-associated mitochondrial import and export pathways in trypanosomes and anaerobic protists. *Eukaryot Cell* 12: 343–355.
44. Diamond LS, Clark CG, Cunnick CC (1995) YI-S, a casein-free medium for axenic cultivation of *Entamoeba histolytica*, related *Entamoeba*, *Giardia intestinalis* and *Trichomonas vaginalis*. *J Eukaryot Microbiol* 42: 277–278.
45. Ali V, Hashimoto T, Shigeta Y, Nozaki T (2004) Molecular and biochemical characterization of D-phosphoglycerate dehydrogenase from *Entamoeba histolytica*. A unique enteric protozoan parasite that possesses both phosphorylated and nonphosphorylated serine metabolic pathways. *Eur J Biochem* 271: 2670–2681.
46. Ali V, Shigeta Y, Nozaki T (2003) Molecular and structural characterization of NADPH-dependent d-glycerate dehydrogenase from the enteric parasitic protist *Entamoeba histolytica*. *Biochem J* 375: 729–736.
47. Olson JW, Agar JN, Johnson MK, Maier RJ (2000) Characterization of the NifU and NifS Fe-S cluster formation proteins essential for viability in *Helicobacter pylori*. *Biochemistry* 39: 16213–16219.
48. Sambrook J, Fritsch EF, Maniatis T (2001) *Molecular Cloning: a Laboratory Manual*, 3rd edn. Cold Spring Harbor: Cold Spring Harbor Laboratory Press, 2001.
49. Roy A, Kucukural A, Zhang Y (2010) I-TASSER: a unified platform for automated protein structure and function prediction. *Nat Protoc* 5: 725–738.
50. Eswar N, Webb B, Marti-Renom MA, Madhusudhan MS, Eramian D, et al. (2007) Comparative protein structure modeling using MODELLER. *Curr Protoc Protein Sci Chapter 2: Unit 2.9*.
51. Laskowski RA, MacArthur MW, Moss DS, Thornton JM (1993) “PROCHECK: a program to check the stereochemical quality of protein structures.” *J Appl Crystallog* 26: 283–291.
52. Eramian D, Shen MY, Devos D, Melo F, Sali A, et al. (2006) A composite score for predicting errors in protein structure models. *Protein Sci* 15: 1653–1666.
53. Ewald PP (1921) “Die Berechnung optischer und elektrostatischer gitterpotentiale.” *Annals of Physics* 369: 253–287.
54. Srinivasan K, Stalin T, Sivakumar K (2012) Spectral and electrochemical study of host-guest inclusion complex between 2,4-dinitrophenol and beta-cyclodextrin. *Spectrochim Acta A Mol Biomol Spectrosc* 94: 89–100.
55. Sharma A, Nigam A (2010) Structure modeling of novel DNA glycosylase enzyme from oral pathogen *Streptococcus sanguinis*. *Bioinformation* 5: 136–140.
56. Subramaniam S, Mohammed A, Gupta D (2009) Molecular modeling studies of the interaction between *Plasmodium falciparum* HslU and HslV subunits. *J Biomol Struct Dyn* 26: 473–479.
57. Nachin L, Loiseau L, Expert D, Barras F (2003) SufC: an unorthodox cytoplasmic ABC/ATPase required for [Fe-S] biogenesis under oxidative stress. *EMBO J* 22: 427–437.
58. Dean DR, Bolin JT, Zheng L (1993) Nitrogenase metalloclusters: structures, organization, and synthesis. *J Bacteriol* 175: 6737–6744.
59. Leippe DD, Wolf YI, Koonin EV, Aravind L (2002) Classification and evolution of P-loop GTPases and related ATPases. *J Mol Biol* 317: 41–72.



